Advanced Materials Technologies

ADVANCED MATERIALS TECHNOLOGIES
www.advmattechnol.com

REVIEW OPEN ACCESS

Lattice Structures for Bone Replacement: The Intersection of Bone Biomechanics, Lattice Design, and Additive Manufacturing

Stylianos Kechagias[1,2] | Maxwell J. Munford[1,3] | Frederik C.H. Masure[1,3] | Richard J. van Arkel[1] | Reece N Oosterbeek[4]

[1]Department of Mechanical Engineering, Imperial College London, London, UK | [2]Department of Mechanical, Manufacturing & Biomedical Engineering, School of Engineering, Trinity College Dublin, Dublin, Ireland | [3]OSSTEC Ltd., London, UK | [4]Department of Engineering Science, University of Oxford, Oxford, UK

Correspondence: Reece N Oosterbeek (reece.oosterbeek@eng.ox.ac.uk)

Received: 4 September 2025 | **Revised:** 18 December 2025 | **Accepted:** 19 December 2025

Keywords: additive manufacturing | lattice structures | orthopedic implants | osseointegration | post-processing

ABSTRACT

Additive manufacturing (AM) has enabled the development of highly porous orthopedic implants by incorporating lattice structures that mimic the micro-architecture of natural bone. Lattices can be tuned to replicate bone's mechanical properties, creating implants that preserve the bone environment and allow bone formation within lattice pores. This review examines the intersection of bone biology, lattice design, and AM technologies to guide the development of such biomimetic structures. The hierarchical structure, mechanical properties, anisotropy, and heterogeneity of bone are identified as critical factors influencing bone remodeling, which is regulated by mechanical stimuli and can inform lattice design. Lattice mechanical behavior can be tailored through base material, relative density, topology, anisotropy, and size, which in turn affect biological responses, including cell function, tissue growth, and vascularization. Among available AM methods, powder bed fusion demonstrates the greatest capacity for producing complex geometries with high precision and reproducibility. Post-processing techniques, such as surface and thermal treatments and biomimetic coatings, are increasingly recognized as crucial for enhancing mechanical and biological performance. Still, current clinical and preclinical applications underscore remaining challenges in improving fatigue life, implant stabilization, vascularization, and bioactivity. This review provides a framework for advancing the design and clinical translation of lattice-based orthopedic implants.

1 | Introduction

Degenerative diseases like osteoporosis and osteoarthritis are prevalent health conditions and one of the primary causes of disability worldwide. Osteoarthritis currently affects over 7% of the global population [1]. While this is typically attributed to ageing populations, early-stage osteoarthritis is increasingly affecting adults of working age due to joint injuries, obesity, and

Abbreviations: AI, Artificial Intelligence; AM, Additive Manufacturing or Additively Manufactured; ASTM, American Society for Testing and Materials; BCC, Body-Centered Cubic; BJT, Binder Jetting; CAD, Computer-Aided Design; CE, Chemical Etching or Chemically Etched; CP-Ti, Commercially Pure Titanium; CT, Computed Tomography; DED, Directed Energy Deposition; EBM, Electron Beam Melting; ECM, Extracellular Matrix; ELI, Extra Low Interstitial; FCC, Face-Centered Cubic; FDM, Fused Deposition Modelling; FFF, Fused Filament Fabrication; FEM, Finite Element Modelling; HIP, Hot-Isostatic Pressing; HT, Heat Treatment or Heat Treated; ISO, International Organization for Standardization; MEX, Material Extrusion; MJT, Material Jetting; PBF, Powder Bed Fusion; PEEK, Poly-Ether-Ether-Ketone; PROM, Patient Reported Outcome Measures; RGD, Arg-Gly-Asp tripeptide sequence; SEM, Scanning Electron Microscopy; SL, Sheet Lamination; SLM, Selective Laser Melting; SLS, Selective Laser Sintering; TPMS, Triply Periodic Minimal Surfaces; VEGF, Vascular Endothelial Growth Factor; VPP, Vat Photopolymerization; µCT, Micro Computer Tomography.

congenital aberrant bone shape [2]. Musculoskeletal conditions are associated with long-lasting pain and disability, impacting people's ability to work and live an active, healthy life. The most common treatment constitutes joint arthroplasty, where worn cartilage and bone sections are replaced by synthetic implants, with the goal of restoring functionality and improving the quality of life for affected individuals.

Traditionally, arthroplasty implants relied heavily on acrylic cement to stabilize and fix the implant within the bone. This technique is cost-effective and has satisfactory survivorship [3]. The drawbacks of cemented implants are extended operation time, cement fragmentation, and aseptic loosening. The latter is caused by cement fatigue and requires treatment with revision surgery [4]. In other cases, there are concerns about post-operative cardiovascular complications such as vasodilation and inflammation of the implant site associated with patients' bone quality and age, or excessive use of cement [5].

In recent years, arthroplasty has shifted away from cemented implants toward cementless alternatives. Bone is a tissue with high regenerative capacity, manifested as a healing response after injury and continuous remodeling throughout adult life [6]. In this context, cementless surgery aims to generate long-term fixation via osseointegration, whereby bone grows onto and into the implant for a direct functional attachment to the implant. Owing to the cement's absence, intraoperative and short-term post-operative implant fixation relies on friction, achieved via a tight press-fit of the implant inside the host bone. Design features like pegs can improve fixation, and screws can be added depending on the anatomical site [7–9].

The first generation of cementless implants had roughened surfaces generated through plasma spraying and grit blasting [10, 11] or by the attachment of metallic beads [12] and fibre meshes [13] to provide a surface texture that favors bone attachment and growth, and improved initial fixation by increasing friction with bone [14]. These approaches are characterized by low porosity, where osseointegration is limited to the interface between bone and implant (bone ongrowth), and in rare cases, this can lead to failure with large loads [15, 16]. In addition, the rough "coating" layer is usually not strongly attached to the implant surface, and under the effect of repeated loading, it can delaminate [17, 18].

Orthopedic implants were historically fabricated using machining, forging, or casting, constituting solid metallic parts made of titanium or cobalt-chrome alloys that have a modulus of elasticity orders of magnitude (10 to 100 times) greater than natural bone. The result is an implant that is typically stiffer than the bone it has replaced, thus changing the load transfer to bone [19]. As bone is a dynamic material that remodels in response to its mechanical loading (Wolff's law) [20], this can lead to regions of bone that are 'stress-shielded', resulting in lost bone mass and, in extreme cases, even periprosthetic fracture [21]. Aseptic loosening is the leading cause of failure in cementless surgeries [22], and periprosthetic fracture remains one of the most challenging to treat.

Additive manufacturing (AM) technology has revolutionized the design of cementless orthopedic implants by enabling the manufacture of complex porous structures with intricate shapes. Made using the same metallic materials, these structures can be designed to lower stiffness to improve load transfer to bone, whilst maintaining acceptable implant strength for withstanding physiological loads [23, 24]. Additionally, unlike previous cementless surfaces, 3D-printed porous structures exhibit high porosities with distinguishable pores, allowing cells from the host bone to migrate and form a new extracellular matrix (ECM) within these pores [16]. In this case, osseointegration is referred to as bone ingrowth, which promises mechanically superior fixation owing to the higher surface area at the interface of bone and implant.

Cementless surgery relies on the longevity of the bone-implant interfacial connection and has become increasingly popular for treating active and working-aged patients who exhibit higher-than-average failure rates with cement fixation [25]. Still, the musculoskeletal treatment of active and working-age patients remains a great challenge for healthcare worldwide. Despite the effectiveness of initial surgical procedures, the rate of revision surgeries for this particular patient group is more than 35% [26]. These outcomes not only harm patients' lives but also pose a huge economic burden on national healthcare systems, as revision surgeries require longer hospitalization and higher costs than the initial surgeries [27].

The success of cementless implants hinges on their ability to promote active bone remodeling and osseointegration with mature bone tissue formation, while providing sufficient mechanical endurance to support physiological loading. The emergence of additive manufacturing for the development of highly porous cementless implants holds promise for enhanced osseointegration and reduced revision rates, allowing patients to live an active life after surgery. This underscores the need for material design and manufacturing that support and accelerate this natural healing process. This review seeks to provide a comprehensive overview of the key requirements for next-generation porous orthopedic implants, emphasising biomimicry, the interplay between lattice micro-architecture and mechanical properties, and also addresses manufacturing and post-processing challenges inherent to additive manufacturing techniques.

2 | Understanding Bone for Biomimicry

During joint arthroplasty, surgeons remove the damaged or deteriorated cartilage, exposing the underlying bone. The exposed bone serves as the foundation for the implant, providing the necessary support and fixation. Consequently, the longevity and success of cementless implants depend on preserving bone health through bone remodeling as well as the successful osseointegration.

Implants with properties designed to control bone mechanobiology could be particularly useful for: (a) accelerating the rate of tissue regeneration/bone ingrowth, (b) enabling early intervention treatments that are likely to be revised in the patient's lifetime, or (c) overcoming longer-term challenges such as stress shielding. Subsequently, the design of biomimetic materials seeking to replicate bone's strain response must be informed by a refined understanding of bone's remodeling response, structure, and mechanical heterogeneity.

2.1 | Bone Remodeling and the Mechanical Environment

Bone's remodeling response and adaptation are closely influenced by the strain (ε) it experiences. This involves the cross-talk between bone's three major cell types: the osteocytes, which sense mechanical stimulation and convert it to biochemical signals; osteoclasts, which are instructed by these biochemical signals to break down old or damaged bone (resorption); and osteoblasts, which rebuild it (apposition) [28]. Resorption tends to dominate at strains below 0.005% (50 $\mu\varepsilon$), indicating bone disuse and reduction in bone density [29]. A homeostatic equilibrium occurs at strains between 50 and 1000–1500 $\mu\varepsilon$, where the amount of bone lost during resorption will be replaced with new bone during apposition with no significant change in bone mass. At higher strains, bone formation predominates, leading to an increase in bone mass due to the deposition of lamellar bone and minerals [29, 30]. However, when the strain becomes excessive, woven bone begins to form. Although no definitive threshold for woven bone formation has been established, different studies suggest it occurs within the range of 2000 $\mu\varepsilon$ [29] to 4000 $\mu\varepsilon$ [30], with deviations that may occur due to load frequency, magnitude, and local bone apparent modulus. The tensile yield strain of bone fractures is around 6500 $\mu\varepsilon$ (0.65%) [31].

By taking into consideration these observations on active bone remodeling, cementless implants should be designed to harness bone's natural mechanoresponse by invoking a localized increase in strain to maintain or improve the quality of the bone in which they are placed. A physiological range of bone strain (approx. 50 to 4000 $\mu\varepsilon$) exists where bone formation can be controlled for mechanical gain (Figure 1a), which can be achieved if the apparent modulus of the implant matches that of the host bone.

An additional challenge during osseointegration is the movement of the implant relative to the bone. Strong osseointegration can take several months, and during that time, the implant is dependent on mechanical friction to remain stable inside the bone. Minimizing implant micromotion is crucial for successful osseointegration. Appropriate values of micromotion can range from tenths to hundreds of micrometres depending on loading time, implant type, and material. The limit of tolerable micromotion has been reported in the range of 15 to 750 μm, averaging 112 μm [32]. Implants with bone-matching stiffness can yield a more homogeneous stress distribution with physiological stress values compared to stiff implants, and while micromotion around low-stiffness implants may increase, it remains within a range that enables osseointegration [33].

Bone is a material with high structural hierarchy, leading to deviations of its apparent modulus depending on anatomical site, age, sex, nutrition, activity level, and bone health [34]. In order to control localized bone strain, it is therefore necessary to understand the heterogeneity and anisotropy of bone's apparent modulus.

2.2 | Bone Hierarchical Structure

Mature bone demonstrates two distinct types: the cortical (compact) and the cancellous (trabecular). The cortical bone is the outer dense layer, with porosity between 3% and 12%, and an average density of 1.80 g/cm^3. The cancellous bone is the inner part that distributes joint loads to the cortex and allows for the transportation of nutrients, minerals, and cells within its pores [35]. Its porosity ranges from 50% to 90%, with an average density of around 0.2 g/cm^3. Both bone types appear as a composite made up of an organic matrix, primarily consisting of collagen type I, interspersed with mineral crystals – mainly calcium apatites in the form of hydroxyapatite [36].

In cortical bone, multiple lamellae (i.e., mineralized collagen sheets) are arranged concentrically around a central canal (the Haversian canal). This cylindrical unit is known as the osteon and exhibits a diameter between 200 and 250 μm [35]. Cortical bone is formed by osteons arranged in parallel, with distinct boundaries defined by cement lines. The Haversian canals run longitudinally through the bone and enclose blood vessels, nerves, and lymphatic vessels. Additional canals (Volkmann's canals) are oriented transversely to osteons and act as links between the inner part of bone and larger arteries, veins, nerves, and lymphatic vessels around it [37]. The cancellous bone consists of a network of interconnected rods and plates, called trabeculae, which are formed by lamellae oriented in parallel, resulting in a thickness of about 50–300 μm [35, 38]. The voids formed (pores) between trabeculae exhibit random shapes and distribution, with their size found to range between 300 and 2000 μm [39, 40] and are filled with red bone marrow and blood vessels [41].

While cortical bone demonstrates superior mechanical properties owing to its high density, the cancellous bone comprises a highly efficient design that combines high compressive strength with low weight and stiffness. This has inspired the development of synthetic porous structures that mimic the trabecular network and offer mechanical properties similar to natural bone.

2.3 | The Apparent Modulus in Bone

Major mechanical properties, such as compressive strength and the apparent elastic modulus, are proportional to bone density, which in turn can be inferred from computed tomography (CT) scans. This allows the estimation of bone mechanical properties in vivo and non-destructively for use in analysis and implant design. The difference in porosity between the two bone types, as well as porosity gradients within the same bone type, results in a wide range of apparent elastic moduli, spanning 7–30 GPa in cortical bone and 0.05–5 GPa in trabecular bone [34, 42]. During joint arthroplasty, however, the trabecular bone is the one being primarily exposed and hosts the implant; thus, for biomimicry, an implant would need to match the stiffness of trabecular bone.

While it is widely accepted that bone density is linked to strength and modulus, the exact relationship depends on the anatomic site. Inter-site differences and intra-site differences for bone properties have been reported to vary by up to 65% and 50%, respectively [42]. As a representative example, bone of a given density has a greater apparent modulus in the tibia compared to vertebral bone and in the femoral neck [42]. Such results indicate that there is no universal model or range of values for bone apparent modulus that can be used when designing implants. It

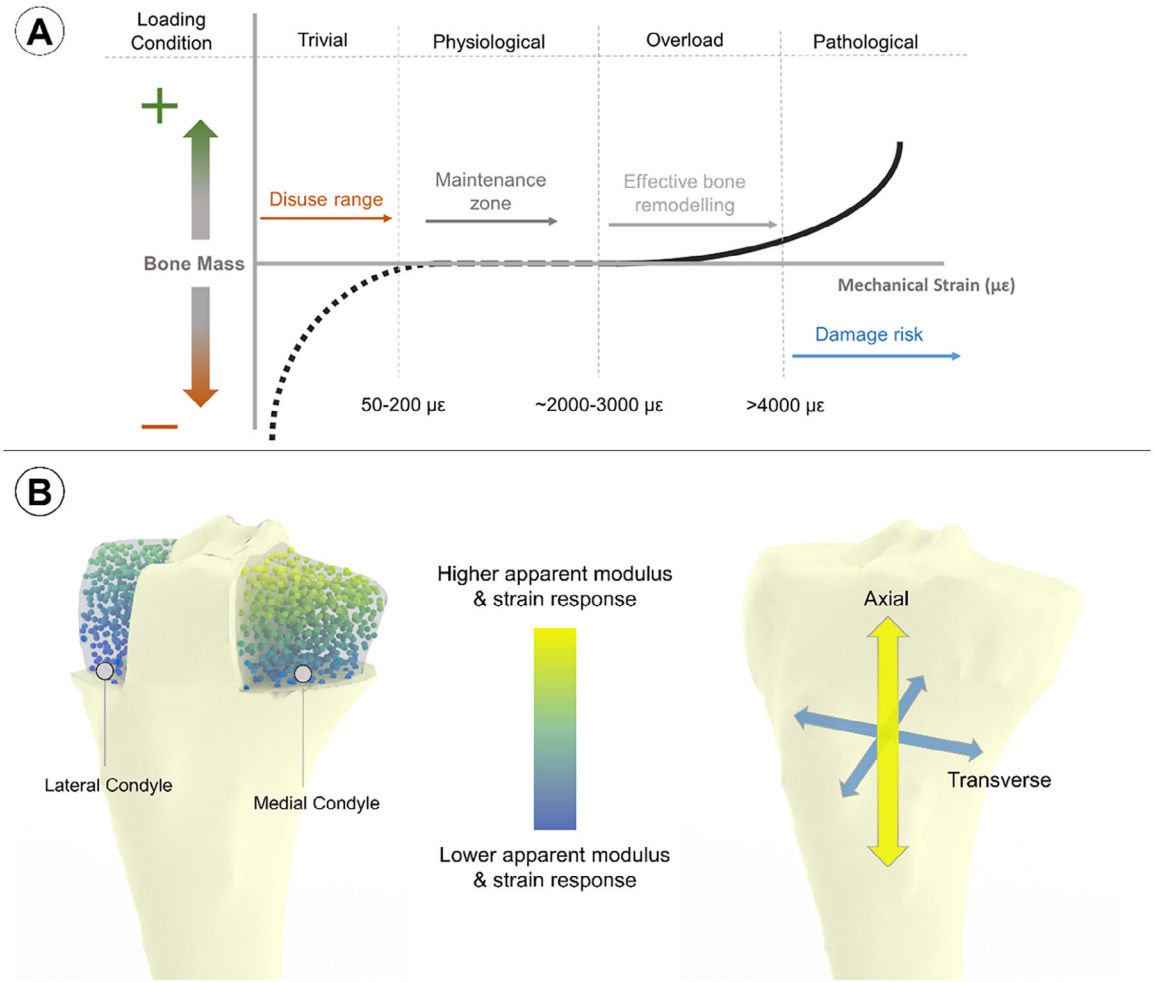

FIGURE 1 | Mechanoregulation and local anisotropy in bone as design cues for orthopedic implants. (A) Relationship between mechanical strain and bone mass adaptation. Bone resorption predominates under low mechanical loading (disuse range), while bone formation dominates under high loading (overload range). A physiological maintenance zone exists between these extremes, where bone turnover remains balanced. Values based on [29, 30, 73]. (B) Spatial distribution of apparent modulus and strain response across the proximal end of a right-sided tibia, showing the medial and lateral tibial condyles. Higher apparent modulus and strain response are indicated in yellow, lower in blue. In the anatomical standing position, the medial condyle lies toward the midline of the body, and the lateral condyle lies on the outer (lateral) side. The right panel illustrates the principal material orientations of trabecular bone, with arrows indicating the axial (proximal–distal) and transverse (medial–lateral and anterior–posterior) directions.

is therefore useful to focus on a specific region of bone and how variation in bone mechanical properties can be accounted for.

The proximal tibia is an example of an anatomical site where refined knowledge of mechanical properties is of particular interest. This is motivated by the global use of knee arthroplasty procedures (millions per annum), which can lead to periprosthetic bone loss and aseptic loosening; indeed, loosening of the tibial component is the primary reason for revision following total knee arthroplasty (TKA) [22]. Sources in literature have reported axial apparent modulus of trabecular bone ranging from 2.5 to 3780 MPa [43–49] and can yield variations in apparent modulus prediction of a factor of 15 even within the same anatomical site of the proximal tibia. Variation between studies may be due to donor, storage methods, sample extraction, imaging methods, or testing protocol.

In addition, relatively few studies have mapped apparent modulus and strength differences in regions across the tibial cancellous bone. Existing data suggest that the modulus changes across the proximal tibia, reaching a maximum in the medial condyle; an intuitive finding given the uneven mediolateral load distribution in the knee due to the knee adduction moment during gait. Trends in literature values for peak medial-lateral ratio (averaged over all depths) have been reported at 1.7 [46, 50], 1.1 [51], and 1.4 [47]. Odgaard et al. observed significant inhomogeneity in axial strain within trabecular specimens under compression, with the intermediate third deforming less than the proximal and distal ends, indicating local gradients in apparent modulus as observed elsewhere in the literature [52]. Similarly, others have found a decrease in axial apparent modulus moving distally [44, 49, 51, 53]. Differences have also been quantified between medial and lateral condyles and subchondral depths. Trends in the literature suggest that the axial apparent modulus is greater in the medial condyle than in the lateral condyle and that the axial apparent modulus is significantly greater than in either of the transverse directions (Figure 1b). This is consistent with Wolff's law and bone remodeling theory as the knee adduction moment during

activities such as gait means that medial loading is typically higher [20, 44, 45].

The proximal tibia exemplifies the intricate spatial and directional variations in bone mechanical properties. Similar complexities are observed in other load-bearing joints. For instance, the acetabulum on the hip exhibits significant regional differences in subchondral bone density, with higher values in the superior region compared to the inferior, reflecting asymmetrical joint loading during activities like walking and stair climbing. Additionally, the trabecular architecture in the acetabulum aligns with principal stress directions, indicating adaptation to habitual loading patterns [54]. In the calcaneus (heel bone), studies have shown that during walking, the bone bears approximately 50% of body weight during the heel strike to midstance phases, leading to regional variations in bone structure. These examples underscore that variations in bone modulus are not unique to the knee but are widespread across load-bearing bones, influenced by complex mechanical stimuli. To accurately replicate these spatially variable properties in implants, it is essential to have precise control over mechanical behavior across different positions, depths, and loading directions – a capability achievable through advanced additive manufacturing techniques [55].

2.4 | Prediction of Apparent Modulus

Measuring the mechanical properties of bone is made difficult given its mechanical and structural heterogeneity [48]. With such complex behavior, it is useful to be able to simply express mechanical properties as a function of density, accounting for spatial variation and whether the bone is trabecular or cortical [56]. Many authors seek to establish a relationship whereby density and apparent modulus can be predicted from imaging methods [42]. It is well understood that the apparent modulus E of a porous material is related to its density ρ via a power law relationship:

$$E = A\rho^B \tag{1}$$

Techniques such as CT scanning can be used to measure density, as X-ray attenuation is directly related to physical density – denser regions absorb more X-rays, resulting in higher grayscale values. These values can be calibrated to estimate local and bulk density for mechanical property prediction.

Although the most common method of predicting mechanical properties is from CT imaging, some studies, such as those by Johnston et al., Nazemi et al., and Ashman et al., have found apparent modulus from alternative methods such as indentation testing, finite element modelling (FEM) combined with neural networks, or ultrasound testing. In all cases, the range of results is similar regardless of testing methods, although values from Nazemi et al. and Ashman et al. were slightly less and greater, respectively, than those results for prediction from CT imaging [49, 57, 58].

Recent data have also shown that an improved prediction of apparent modulus can be made if precise anatomical location is accounted for: models that account for spatial heterogeneity account for 31% more variation in apparent modulus than other models [53].

It must be noted that there are limitations to using CT imaging for mechanical property prediction. Factors such as bone collagen content, gait, and diet affect these properties and are not captured with CT imaging. Similarly, bone apparent density, trabecular volume, apparent modulus, strength, and strain energy are all affected by medication, which literature models do not capture. Furthermore, bone's ability to remodel changes with protein content and age, as osteocytes become senescent, which is likely to further contribute to the variation in properties observed in the data here [59]. Finally, clinical CT does not image with sufficient resolution to capture structural anisotropy or microcracks [60], only gross density changes.

2.5 | Considerations on Anisotropy

Mechanical anisotropy in bone (i.e., exhibiting directionally dependent properties) has been associated with the alignment of trabeculae with respect to the loading direction (structural anisotropy). Isotropic materials have equal properties in all three principal directions, anisotropic materials have different properties in their three principal directions, and orthotropic materials are a special case of anisotropic materials and have properties described by a principal axis and approximately equal properties in the two transverse directions (Figure 1b) [61].

In regard to mechanical properties, most studies have assumed isotropic properties for bone; however, some studies suggest that an orthotropic relationship is more suitable. The orthogonal properties of the proximal tibia are well characterized [49, 51, 53, 62–64]. Apparent modulus in the transverse directions is reported between 51 and 553 MPa with a degree of anisotropy ($E_{max,principal}/E_{min,principal}$) ranging from 1.1 to 4.3. However, modulus variation across the tibial plateau has not been specifically analysed, despite its potential impact on calculating load distribution, implant design, or surgical planning. Anisotropy has also been shown to be greater on the medial side than the lateral side (1.9 compared to 1.4) and also to decrease with subchondral depth [46].

Quantifying structural anisotropy relies on high-resolution micro-CT scans, followed by the calculation of a mathematical tool known as the fabric tensor. This tensor describes how the structural elements within a porous material – such as trabeculae in bone – are oriented in space. It is typically a second-order symmetric tensor, which captures orientation patterns in three dimensions [61]. The fabric tensor can be calculated using computational methods such as the mean intercept length, volume orientation distribution, or star volume distribution [65]. Based on the directions and alignment of the trabeculae, the tensor highlights the main structural directions and how much material is oriented along each one. It can be visualized as an ellipsoid with three principal axes (derived from fabric eigenvalues) [65]. The fabric eigenvalues are used for calculating the degree of anisotropy (ratio of highest to lowest eigenvalues) [66] while the shape of the ellipsoid indicates any preferential orientation of the structure: a more elongated ellipsoid means a highly

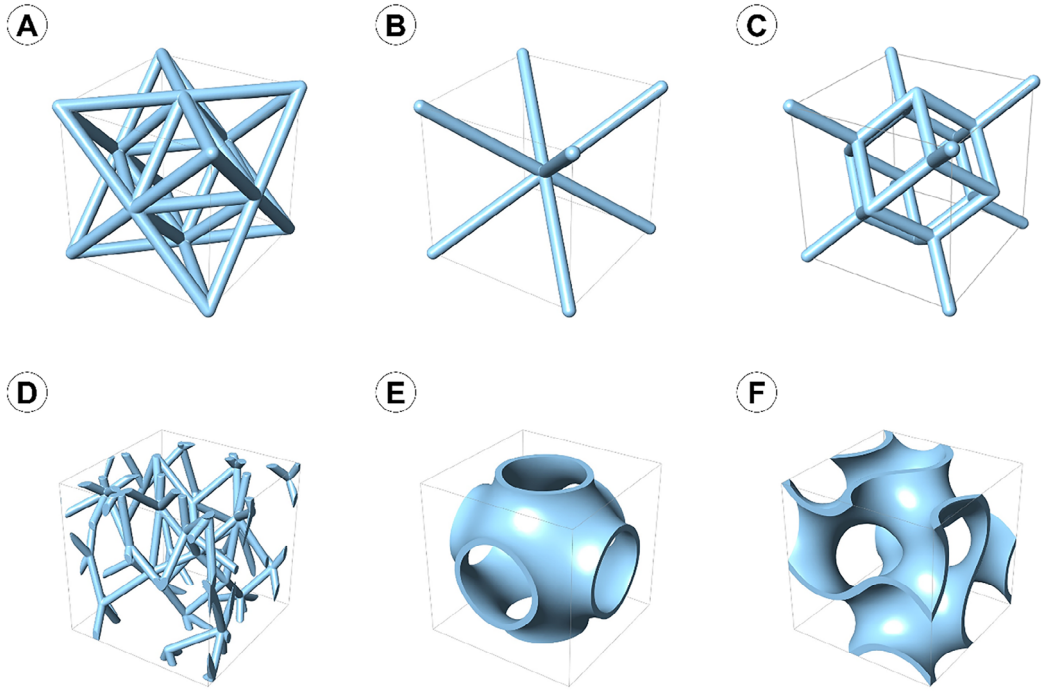

FIGURE 2 | Examples of lattice structures. Strut-based (A) octet-truss, (B) body-centred cubic, (C) dodecahedron, and (D) stochastic structures. Sheet-based (E) Schwartz primitive and (F) Schoen gyroid.

oriented structure (high degree of anisotropy), while a more spherical ellipsoid means a more isotropic structure (low degree of anisotropy) [67].

In the case of the proximal tibia, past works have used μCT scans to quantify anisotropy through micro-FEM and fabric methods, with results obtaining an average anisotropy between 1.3 and 2.8 [68–71], agreeing broadly with results from mechanical testing. The close alignment of fabric methods and mechanical analyses has led authors to suggest that anisotropy in the mechanical properties of bone correlates with micro-CT-derived fabric tensor data [65, 72].

3 | Design Concepts and Mechanical Properties of Lattice Structures

3.1 | Biomimetic Designs

Biomimicry requires control of material properties in porous structures. The first generation of such synthetic structures was developed by liquid-state processes (e.g., foaming through gas injection or casting) and solid-state processes (e.g., powder sintering using space holders or hollow microspheres), generating foams with open or closed interconnected pores made of metals, polymers, ceramics, and ceramic-polymer composites [74–76]. While tuning of the respective process parameters can lead to controlled porosity and pore size/shape, the above methods result in randomly distributed pores, which greatly compromise the mechanical performance and impede reproducibility. Additive manufacturing arose as a promising alternative allowing more precise control over structure morphology, scalability, and complexity. In the context of additive manufacturing, these porous structures are termed lattices and constitute 3D networks of struts (i.e., beams) or sheets (i.e., plates) and can utilise periodic or stochastic (randomized) micro-architecture [77].

Periodic lattice structures consist of geometrically defined and spatially repeating unit cells. In the case of strut-based lattices, unit cells are typically designed to represent crystal structures (e.g., the body-centred cubic and face-centred cubic) (Figure 2a,b), or Platonic and Archimedean polyhedra [78] (Figure 2c). In the case of sheet-based lattices, unit cells are designed based on triply periodic minimal surfaces (TPMS), such as the Schwartz primitive and Schoen gyroid (Figure 2e,f), which are smooth and infinitely repeating surfaces creating a boundary between solid and void sections of the structure [77, 79].

Stochastic lattice structures can be both strut-based and sheet-based. Strut-based stochastic structures are typically generated by connecting randomly distributed points derived from statistical distributions (e.g., Gaussian and Poisson) or the edges of the Voronoi diagrams [80–82] (Figure 2d). Similarly, sheet-based stochastic structures can be generated by segmenting a 3D volume into randomly shaped subregions, which are then represented with randomly oriented periodic TPMS [83] or randomly defined surfaces [84]. Alternatively, randomized sheet-based structures can be designed as spinodoid metamaterials, which mimic spinodal decomposition and feature smooth, non-intersecting, and bi-continuous surfaces that minimize stress concentrations and exhibit enhanced resistance to failure due to their lack of symmetry-dependent weak points [85]. These structures offer highly tunable anisotropy, and recent studies have demonstrated that, by integrating AI-driven design frameworks, they can be tailored to closely replicate the anisotropic mechanical behavior of cancellous bone [86].

All the above methods enable the creation of pseudo-random structures: a structure that appears random, but can be replicated with a controllable micro-architecture. This is achieved by generating random points from seed numbers, which allows the reproduction of the same lattice at any time. This capability is a significant advantage over early forms of synthetic foams, where micro-architecture was inherently less controllable and reproducible.

Each lattice type incorporates distinct advantages and disadvantages, making the selection of a lattice highly dependent on the specific application. Periodic structures offer more predictable mechanical behavior owing to their regular and repetitive micro-architecture. They have also been shown to exhibit superior mechanical properties than stochastic lattices for both strut-based [87] and sheet-based [83] structures. This is often attributed to the randomness of stochastic structures, which can introduce weak (less supported) regions inside the specimen [88]. From a design point of view, though, stochastic designs benefit the fabrication of lattice-based parts with irregular or curved geometry. While stochastic structures can easily represent such geometries by relying on randomly populated points, periodic structures rely on computational algorithms to change the size/shape of their unit cells and conform them to the part's external surface [89, 90]. Stochastic structures may also be advantageous for bone as optimum parameters are not precisely known and will vary from person to person: the stochastic structure provides, to some extent, a "spread-bet" of slightly varying properties and pore sizes within the relevant range.

Sheet-based lattices are often recognized for their superior mechanical properties, which are attributed to their smoother surface transitions leading to lower stress concentrations [91–94]. The continuous nature of these surfaces leads to more uniform stress distribution, reducing the likelihood of localized stress concentrations that can occur in strut-based lattices. In contrast, the discrete nature of strut-based lattices can result in stress concentrations at strut junctions, making these structures more sensitive to local defects and introducing anisotropic behavior. However, strut-based lattices are generally easier to design and more straightforward to manufacture, especially in the case of additive manufacturing. Due to their complex geometries and large surface areas, sheet-based lattices often require additional support structures to manage overhanging surfaces and prevent warping during fabrication. Furthermore, the large surface area in sheet-based lattices can lead to higher entrapped porosity and potential defects due to excessive local energy deposition during additive manufacturing [92].

A comparison of different lattice types is summarized in Table 1.

3.2 | Mechanical Performance under Quasi-Static Loading

3.2.1 | Main Factors for Controlling Mechanical Properties

The mechanical performance of synthetic cellular materials primarily depends on three factors: the base material, the relative density, and the topology.

The base material dictates the intrinsic mechanical behavior and properties, such as strength, stiffness, ductility, and toughness. The ductile or brittle nature of the base material is particularly critical in determining how a porous structure responds to mechanical loads [88]. Ductile materials like polymers and most metals allow structures to deform plastically under load, with their struts/sheets undergoing extended bending or buckling. In contrast, porous structures made from brittle materials like ceramics, although exhibiting high stiffness and strength, are more prone to catastrophic failure without significant plastic deformation due to sudden fracture of their struts/sheets. These differences are also apparent for the same material type. For example, commercially pure titanium (CP-Ti) is known to be more ductile than the alloy Ti-6Al-4V, and so while it has lower ultimate tensile strength, it is capable of undergoing higher plastic deformation without fracture [95].

Relative density is defined as the ratio of a structure's apparent density ρ to the density ρ_s of the base material. Gibson and Ashby [96] proposed a generalised power-law relationship to correlate relative density with the edge length L and the strut/sheet thickness t of a structure's unit cells:

$$\frac{\rho}{\rho_s} \propto \left(\frac{t}{L}\right)^2 \tag{2}$$

Although in this model is derived by assuming any porous structure as a cubic array with unit cell edge L and thickness t, it has been shown to predict relative density for both periodic and stochastic structures with high accuracy. This approximation is practical in the case of stochastic structures where a single pore geometry is difficult to define. However, more detailed analytical expressions correlating relative density with L and t can be derived from the unit cell geometry in regular structures [97].

Relative density is inversely related to the size of the pores and complementary to a structure's open porosity φ (the aggregate volume of voids divided by the structure's volume) and can be expressed as:

$$\frac{\rho}{\rho_s} = 1 - \varphi \tag{3}$$

Drawing an analogy to the mechanical properties of bone and their link to density (Equation (1)), Gibson and Ashby proposed that the two major compressive properties of any porous structure, the yield strength σ_y and the elastic modulus E, are correlated to relative density via power laws:

$$\sigma_y \propto \left(\frac{\rho}{\rho_s}\right)^n \tag{4}$$

$$E \propto \left(\frac{\rho}{\rho_s}\right)^m \tag{5}$$

where power indices n and m have been found to range between 1 to 3 for the majority of experimental data [77]. This set of equations is usually termed the Gibson-Ashby model and has found wide acceptance across industries for predicting the mechanical properties of a designed structure. This is particularly important

TABLE 1 | Comparison of lattice structure types.

Type	Advantages	Disadvantages
Strut-based periodic	• Simple to design and analyze • Predictable mechanical behavior • Easy to control porosity	• Stress concentrations at nodes • Pronounced anisotropy • Less biomimetic morphology
Strut-based stochastic	• Bone-like morphology • High design flexibility • More isotropic properties	• Stress concentrations at nodes • Less predictable mechanical behavior • Challenging to control local porosity
Sheet-based periodic	• Reduced stress concentrations • High specific strength • Well-defined mathematical control	• Sensitive to manufacturing defects • Limited topological randomness (limits biomimicry)
Sheet-based stochastic	• Reduced stress concentrations • High specific strength • Bone-like morphology	• Complex to design and optimize • Less predictable mechanical behavior • Challenging to manufacture

for orthopedic implants, as the most crucial biomechanical property is the stiffness of the structure, which should be tuned to match the stiffness of the bone to be replaced. The values of power indices in the Gibson-Ashby model are strongly dependent on topology – meaning the connectivity and spatial arrangement of struts, and the shape of the unit cell.

Structures with lower connectivity (i.e., fewer struts meeting at each node) have been shown to have lower strength and modulus and higher power indices [88]. This is explained through the Maxwell criterion for beam frames. Based on the number of struts s and nodes j, the Maxwell number M for 3D frames is calculated as $M = s - 3j + 6$. For a high connectivity structure $M \geq 0$, struts experience axial loads (stretch-dominated deformation) and the structure appears rigid as a statically indeterminate frame. While for a low connectivity structure $M < 0$, struts exhibit bend-dominated deformation and the structure appears compliant as a pin-joined mechanism [88] (Figure 3a).

The strut micro-deformation modes have been extensively studied for various periodic unit cell topologies using experimental, computational, and analytical approaches [98, 99]. Using analytical calculations, a nodal connectivity of at least 12 is necessary for 3D periodic structures to be statically indeterminate and stretch-dominated [100]. A similar approach is not feasible for stochastic structures; however, experimental data suggest that increasing connectivity greatly affects the mechanical behavior of stochastic structures, which appear stiffer than low-connectivity structures of the same relative density [101].

A third micro-deformation mode, buckling-dominated, involves elements that exhibit buckling and a sudden loss of load-carrying capacity at a critical stress level, leading to a nonlinear mechanical response. This behavior is not linked to the Maxwell criterion and connectivity. Rather, it is primarily driven by relative density and the arrangement of struts. For instance, rigid polymer and metallic foams fail by buckling when relative density is ≤5% and ≤1%, respectively [88]. This is attributed to the t/L ratio, also known as the slenderness ratio, which informs the propensity of a structural element to buckle, and its threshold value depends on the base material [102]. Alternatively, buckling can occur in unit cell topologies whose structural elements exhibit high alignment with the loading direction. For example, this is the case for the cubic unit cell [103] when loaded normally, where half of the struts are parallel to the load and the other half are vertical to the load.

3.2.2 | Size and Edge Effects

Size and edge effects refer to the phenomena where the mechanical properties of cellular materials are influenced by their dimensions and boundaries. Smaller structures may exhibit different strength, stiffness, and failure mechanisms compared to larger ones due to the influence of increasing surface-to-volume ratio and the amplified influence of structural defects. Edge effects arise from the differences in the mechanical environment experienced by unit cells at or near the boundaries of the material compared to those in the interior.

Size and edge effects usually act synergistically in small-sized specimens, as damaged or free struts at the edges of the small specimens do not contribute to strength by carrying load while they increase the apparent cross-sectional area or moment of inertia of testing specimens [110, 111]. This coupled effect is primarily apparent in metallic foams, which tend to exhibit lower stiffness, compressive strength, and bending strength when specimens are critically small. However, macroscopic properties eventually converge at constant values when the structure is formed by a large enough number of unit cells [112]. Early studies have demonstrated that convergence occurs when the shortest edge of the specimen is composed of at least 5–8 unit cells [113, 114], and the converged properties are referred to as "bulk" material properties.

There are, however, cases where small specimens may exhibit higher mechanical properties than large specimens. This is often linked to the brittle nature of the base material and the increasing

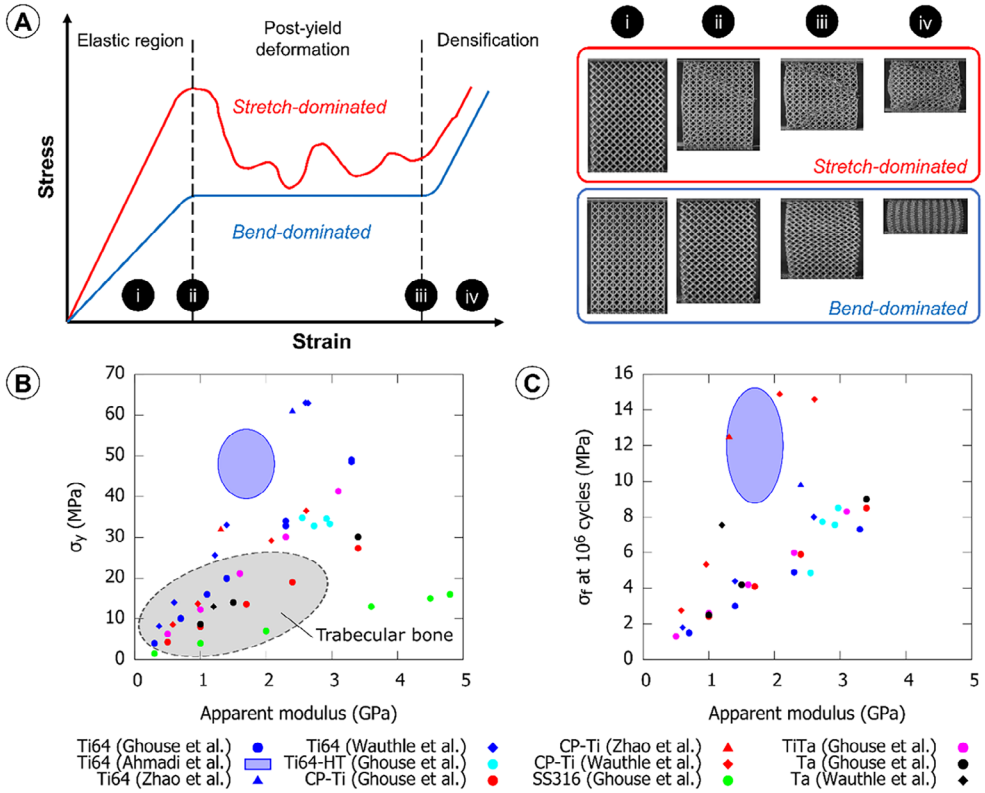

FIGURE 3 | Mechanical performance of lattice structures. (A) Typical shape of stress-strain curves for structures experiencing stretch- and bend-dominated micro-deformation mode. Photographs showing the macroscopic failure of stretch-dominated (FCC-Z) and bend-dominated (BCC) structures. Photographs correspond to strains at the (i) elastic region of the curve, (ii) the initial collapse after yield, (iii) the end of post-yield deformation, and (iv) denfication. Bend-dominated structures tend to collapse uniformly, leading to a barrel shape, while stretch-dominated structures tend to collapse heterogeneously with the formation of a shear band. Both structures were made of Inconel 625 and designed with cubic 2-mm unit cells. Photographs of specimens were reproduced with permission [104]. Copyright 2018, Elsevier. Parameter map showing typically achievable properties from selected literature for additively manufactured lattice structures relevant for bone replacement, from Ghouse et al. [80, 105, 106], Ahmadi et al. [107, 108], Zhao et al. [109], and Wauthle et al. [95]. Showing (B) yield strength (σ_y) and apparent modulus, with approximate values for trabecular bone shown for comparison, (C) fatigue strength (σ_f) for 10^6 cycles and apparent modulus.

number of structural defects found in larger specimens (Weibull theory). More defects and imperfections may lead to randomized fracture of struts at distant regions in larger specimens that will compromise the strength and stiffness compared to small specimens, where defects are statistically fewer [114].

International testing standards for measuring lattice properties (e.g., ISO 13314 and ASTM D1621) assume that the mechanical behavior of a test coupon accurately represents the performance of the structure in its intended application [115, 116]. The standards require coupons to be adequately large (consisting of at least 10 unit cells across the width to avoid size effects) with an aspect ratio (height to diameter/width ratio) between 1 and 2. However, aspect ratios outside this bound have been found to strongly affect the apparent mechanical properties of a lattice structure, depending on whether they are bend- or stretch-dominated [117]. In stretch-dominated lattices, failure often occurs via shear band formation, preserving much of the structure and resulting in higher stiffness at aspect ratios greater than 2 [118]. In contrast, bend-dominated lattices tend to fail through layer-by-layer collapse, which at low aspect ratios (lower than 2) can cause stress concentrations near the platens, limiting uniform strain distribution and increasing stiffness [119]. These observations are important to consider when designing implants with bone-matching properties, as the standardised testing coupons may greatly differ in size and geometry from actual implants.

3.2.3 | Anisotropy in Lattice Structures

Similarly to natural bone, lattice structures can exhibit high anisotropy in their mechanical properties due to their inherently directional architecture. In directions where struts are aligned with the load, the structure typically shows higher stiffness and strength compared to directions where the load is applied transversely to the struts [120]. In lattice structures, the degree of anisotropy can be quantified using μCT data by analyzing the angular distribution of struts, similar to methods used for characterizing bone trabeculae. Alternatively, anisotropy can be assessed directly from computer-aided design (CAD) models by calculating the orientation of individual struts or sheets [121].

A representative example from periodic lattices is the highly interconnected octet-truss lattice, which has been shown to exhibit a yield stress ratio (maximum-to-minimum) of approximately 2 across different loading orientations [122]. Apart from the

property values, though, orientation has been shown to affect the failure mechanism in various lattice topologies such as the cubic and BCC [123, 124]. Non-equivalent deformation of unit cells across different directions can lead to structures having more brittle characteristics, typically associated with stretch-dominated behavior, contrary to what Maxwell's criterion would suggest [125].

These observations have led researchers to manipulate lattice topologies to enhance structures' strength and stiffness along distinct directions. Smith et al. [126] characterized the mechanical behavior of the BCC lattice designed with vertical struts connected to the central node of the unit cell (also called BCC-Z unit cell). In another example, Wang et al. [127] studied the FCC lattice designed by rotating its unit cells to induce different failure mechanisms.

The aspect ratio of the unit cells is another factor that has been shown to greatly affect the mechanical properties and deformation depending on the load direction [126, 128]. Considering a Cartesian coordinate system, more elongated unit cells (or pores) along the Z-axis result in higher compressive strength and higher elastic modulus along Z than X and Y, and a lower Poisson ratio in the XZ and YZ planes.

All the above indicate that anisotropy can significantly impact lattice mechanical performance. In most cases, uniaxial compression tests are inadequate to fully characterize a lattice's behavior in real applications where loading occurs in multiple directions. Another challenge arises from the positioning of a lattice onto an implant's surface, which can exhibit an arbitrary shape and multi-axial loading when inserted into the body. More isotropic lattice topologies can then be beneficial to better predict the mechanical behavior of a structure under multi-axial loading. In this context, periodic structures exhibit a limitation as they often concentrate strength along specific directions aligned with the orientation of their struts. On the contrary, stochastic structures can be designed with struts with a wide angular distribution, leading to a more uniform mechanical response in all directions [129].

3.3 | Mechanical Performance under Dynamic Loading

Lattice structures should be designed with an elastic modulus similar to that of natural bone to enable active bone remodeling. While yield strength is often a factor in material selection, it is not the most essential property for lattice structures in bone implants. Instead, maximizing fatigue strength is critical, as implants must withstand cyclic loading over extended periods. Therefore, optimizing lattice material, processing methods, relative density, and topology is crucial to enhancing fatigue performance and ensuring long-term implant survivorship.

3.3.1 | The Effect of Base Material and Manufacturing Method

Yield strength, ductility, crystal structure (in the atomic level), the presence of multiple material phases, the size and orientation of grains, and the presence of structural defects are widely known to affect the fatigue performance of solid materials [130].

Ductile materials generally have superior fatigue life under high strain amplitudes because of their ability to undergo plastic deformation before crack propagation. In contrast, brittle materials may perform better under low applied strains due to their high yield strength [131]. Nevertheless, the sensitivity of brittle materials to defects limits their extended application in cases that involve cyclic or multiaxial loading, where durability and resistance to crack growth are critical.

Crack propagation can be impeded by inclusions, secondary phases, and grain boundaries, making the size and orientation of grains critical for fatigue strength [132]. Smaller grain sizes introduce a higher density of boundaries that hinder the movement of dislocations within the microstructure, thereby improving resistance to crack initiation and growth. Ultrafine grains (<10 nm), however, will eventually lead to an inverse phenomenon where grain boundary sliding occurs. Depending on the loading direction relative to the grain orientation, materials with a preferred crystallographic orientation (as a result of processing techniques like forging or additive manufacturing) may exhibit a different fatigue response. Grains misaligned with the loading direction may develop higher resolved shear stresses, leading to slipping and promoting early dislocation and crack initiation as described by Schmid's law [133, 134]. Still, grain size stands out as the most influential microstructural factor for fatigue performance compared to orientation [135].

The number of phases present in a material determines the type of microstructure formed, which in turn has a significant impact on fatigue performance. A key example of this relationship is found in titanium and its alloys, which are among the most extensively studied materials due to their widespread use in industries such as aerospace and orthopedics. Major microstructural types include: the equiaxed (typically formed in single-phase materials or after complete recrystallization), the lamellar (two-phased where the phases alternate in a layered arrangement), duplex (a mixture of equiaxed grains and lamellar colonies), and the Widmanstätten (two-phased where one phase appears as needle-like precipitates, typically formed owing to rapid solidification) [136]. The influence of each one in fatigue strength has been investigated thoroughly for both solid and porous forms of titanium [136, 137]. As a representative example for lattice structures, Ghouse et al. [105] compared the fatigue performance of the same lattice made of CP-Ti, Ti-6Al-4V, Ta, and Ti-Ta. They found that Ta and Ti-Ta specimens exhibited the highest fatigue strength at 10^6 cycles over fixed relative density or modulus, which was attributed to better surface quality, higher ductility, and favorable microstructure. Regarding the microstructure, the Ti-Ta was found to exhibit a martensitic $\alpha''+\beta$, which is known to exhibit higher fatigue resistance and decreased notch sensitivity compared to CP-Ti's α phase or Ti-6Al-4V's acicular $\alpha'+\beta$ phase [138]. Similarly, by comparing the same lattice made of CP-Ti and Ti-6Al-4V, Wauthle et al. [95] found that the ductile CP-Ti had better fatigue strength in high-cycle loading (>10^5 cycles), while the brittle Ti-6Al-4V had better performance in low-cycle (<10^5 cycles). These results suggest that a brittle metal with high yield strength may perform better at low-cycle fatigue. Still, in the case of high-cycle fatigue applications where stress is

considerably low, and the yielding effects do not dominate the behavior, ductile metals are favorable. In addition, as discussed later, it underlines the importance of applying post-processing methods such as heat treatment to achieve a more favorable microstructure.

3.3.2 | The Effect of Relative Density

In a similar way to quasi-static strength, higher relative density (i.e., lower porosity) leads to higher (absolute) fatigue strength in porous materials [139]. Due to the interaction of fatigue strength with static strength (Goodman relation), examining the fatigue strength normalized to static strength or modulus can better isolate the true effect of relative density. Hrabe et al. [140] produced Ti-6Al-4V structures with the diamond unit cell, constant strut thickness of ≈400 μm, and relative densities ranging from 17% to 40% by varying the pore size (500–1500 μm). After normalising to yield, the S-N curves showed that structures with higher relative density had also higher fatigue life. The normalized fatigue strength at 10^6 cycles of the lattices ranged from 0.15 to 0.25, while the normalized strength for a solid specimen with the same Ti microstructure was 0.4. The lower normalized fatigue strength in lattices compared to bulk AM parts is expected, as their high surface area-to-volume ratio amplifies the influence of process-induced defects and stress concentrations, accelerating crack initiation and thereby compromising fatigue life. Yavari et al. [141] produced Ti-6Al-4V structures with the dodecahedron unit cell and relative densities ranging from 16% to 32% by altering strut thicknesses (140–250 μm) and pore sizes (500–600 μm). As expected, both the absolute and the yield-normalized S-N curves were more elevated for higher relative density, indicating higher fatigue life.

3.3.3 | The Effect of Topology

Different topologies have also been found to affect fatigue life and strength of lattice materials (Figure 3c). Zhao et al. [142] compared the fatigue behavior of Ti-6Al-4V lattices made with similar relative density, but different unit cells: the buckling-dominated cubic, the bend-dominated G7, and rhombic dodecahedron. Results suggested that the buckling-dominated cubic lattice exhibited a lower rate of cyclic ratcheting and increased fatigue strength (normalised to static plateau stress) than the bending-dominated lattices. This finding was attributed to different internal stresses developed in each case, which are entirely compressive during buckling-dominated deformation and a mix of compressive and tensile during bending-dominated, making the latter more prone to fatigue crack propagation. In line with these results, Peng et al. [143] compared lattices of different unit cells (cubic, BCC, FCC) and relative densities using a computational model and found that the cubic lattice had the highest fatigue strength – both absolute and normalized – while the BCC lattice had the lowest.

Zhao et al. assessed CP-Ti lattices with different unit cells (tetrahedron and octahedron) and pore sizes (500 and 1000 μm), with the high-connectivity octahedron lattices found to exhibit greater fatigue strength than their tetrahedron counterparts at the same pore size [109]. A similar trend was observed in [101], where stochastic lattices with varying connectivities were compared in terms of fatigue life. It was found that increasing strut connectivity, while maintaining a fixed relative density, improved fatigue strength by up to 60%.

In an extensive study, Ahmadi et al. [144] compared lattices built with different materials (CoCr, Ta, Ti64, and CP-Ti), unit cells (truncated cuboctahedron, rhombic dodecahedron, and diamond), and relative densities (ranging from 0.21 to 0.42). When isolating the effect of material, CoCr had the highest normalized fatigue strength, followed by CP-Ti, Ta, and Ti-6Al-4V. However, each material was found to have different sensitivity when altering the unit cell and relative density. Namely, normalized S-N curves for different relative densities of CoCr specimens had no significant difference when made from the diamond unit cell, while showing significant differences when made from the truncated cuboctahedron and the rhombic dodecahedron unit cells. The sensitivity in relative density and topology was lower for the other materials. This was attributed to the post-yielding hardening of bulk CoCr, which results in normalized fatigue strength higher than 1, with the authors concluding that *"as the relative density increases, the fatigue response of porous CoCr structure becomes more similar to the bulk CoCr material and topology contributes less to the fatigue response"*.

Another example of topology investigation comes from Speirs et al. [145] who compared NiTi lattices with the octahedron unit cell and the TMPS gyroid in a cellular and a sheet configuration. All specimens failed with a diagonal shear band formation, but the absolute and normalized fatigue life of sheet and cellular gyroid were significantly higher than the octahedron. The superiority of sheet-based compared to strut-based lattices was also shown in [146], where the sheet-based gyroid was compared to the strut-based FBCCZ (combination of BCC and FCC-Z). Both types exhibited the same relative density and were tested under cyclic tension-compression loading. The study found that the gyroid lattice demonstrated better fatigue life with S-N curves approximating the ones of the solid base material (steel 316L). Both studies concluded that the better cyclic performance of gyroid lattices originates from the lower stress concentration in the nodes compared to the strut-based lattices they were compared to.

4 | Lattice Structures as Scaffolds for Bone Regeneration

When employed in orthopedic implants, lattice structures should combine material properties and topological characteristics that not only provide beneficial mechanical properties but also induce favorable biological function on the tissue and cells that host the implant.

4.1 | Material Selection

The material an implant is made from determines its mechanical properties and biocompatibility. Properties such as elastic modulus, yield strength, fatigue strength, corrosion, and wear resistance not only define the implant's mechanical performance but also its compliance with the environment where it is placed.

From a biological perspective, the base material must be biocompatible for the organism, meaning it does not cause harm or provoke an immune response [15].

Metals are the most widely used materials for orthopedic implants and devices owing to their excellent manufacturability and favorable mechanical properties.

Titanium and its alloys are historically the most commonly used materials for AM porous structures due to their biocompatibility, high specific strength, low elastic modulus, and good corrosion resistance. Titanium-based implants demonstrate sufficient cell adhesion, cell proliferation, and bone in-growth [147]. CP-Ti is advantageous due to its ductile nature (for press-fit applications), absence of toxic alloying elements [148, 149], while as a single-phase metal, CP-Ti demonstrates higher electrochemical corrosion resistance compared to alloys [150]. However, Ti alloys – with Ti-6Al-4V being the most prominent – remain the most widely used in the orthopedic industry due to their well-established manufacturability (e.g., extended use in welding), ample supply of AM powder, high specific strength, as well as heat treatment compatibility due to the additional β-phase. Proper control of the alloy microstructure and heat treatment can improve their ductility while maintaining high strength [106, 151]. CP-Ti and Ti-6Al-4V show similar osseointegration potential; thus, CP-Ti is typically preferred for dental implants due to its superior corrosion resistance, while Ti-6Al-4V is chosen for orthopedic implants for its higher load-bearing capacity [152].

Besides titanium and its alloys, cobalt–chromium–molybdenum (CoCrMo) alloys, stainless steel, and tantalum are widely used in orthopedics due to their distinct mechanical and biological properties. Cobalt-chromium alloys are commonly utilised in joint replacements owing to their excellent wear resistance and strength. Stainless steel (particularly 316L) is often employed in temporary implants like fracture fixation devices because it offers good corrosion resistance and low cost. However, its use in joint arthroplasty has diminished over time because it is less biocompatible and corrosion-resistant than modern alternatives [153]. Tantalum is known for being highly biocompatible, ductile, and corrosion-resistant owing to its ability to form a dense oxide layer, making it a desirable choice in porous implants for bone ingrowth, particularly in spinal fusion and acetabular cups [154].

These metallic materials undergo negligible corrosion and hence will remain permanently installed in the body unless removed due to infection or implant failure. In this regard, magnesium and zinc alloys have recently attracted significant scientific interest as they are biodegradable and can gradually degrade inside the body, eliminating the need for secondary removal surgeries. Both materials offer excellent biocompatibility and low stiffness, promoting bone regeneration during degradation. Common applications include fixation devices for fracture treatment, such as plates, rods, and screws, currently applied for adult patients but with the potential to expand to pediatric patients to avoid disruption of bone growth [155]. Moreover, recent advancements in additive manufacturing have enabled the development of zinc/magnesium-based lattice structures [156, 157], which can now be integrated into medical devices such as screws [158] or act as defect-filling scaffolds [159] for deeper bone ingrowth and vascularization prior to biodegradation. Control of the degradation behavior, so that the implant retains sufficient structural integrity for the duration of healing, is one of the main barriers to the wide adoption of such technology.

Even the most well-established metals in orthopedics have limitations. Released metal ions or particles due to corrosion or wear of alloyed materials – mainly cobalt from CoCr alloys, nickel from stainless steels, and vanadium from Ti alloys [160] – can lead to perilous conditions such as allergic or inflammatory reactions, blood poisoning (metallosis), cytotoxicity, carcinogenesis, and genotoxicity [147, 161]. Up to 12% of patients may have some degree of metal sensitivity, with data suggesting that women may be more affected than men [162, 163]. Even pure metals, such as CP-Ti and Ta, can in certain cases be toxic [148]. However, these materials typically form dense oxide films in contact with air, which are bioinert and in most applications protect the implants from corrosion [15].

In the case of patients with metal sensitivity or severe allergic reactions due to metallic debris release (owing to metal-on-metal contact), revision surgery is performed to replace the metallic components with ceramic-based implants [164, 165]. Although these materials are highly biocompatible, "hypoallergenic" and offer load-bearing capacity, their brittle nature still hinders their extended use in joint arthroplasty due to sensitivity to multi-axial cyclic loading.

4.2 | The Influence of Lattice Micro-Architecture

From a biological perspective, scaffolds should have interconnected open pores with size and shape that favor bone tissue formation and maturation for superior implant-to-bone fixation. Small pores increase the scaffold's surface area-to-volume benefit initially cellular adhesion and later cell communication toward rapid differentiation, tissue formation, and mineralization [166, 167]. Large pores, on the other hand, result in high fluid permeability allowing deep cell migration, oxygen and nutrient transportation, aiding tissue in-growth and vascularization in large-sized implants [168, 169]. Pore sizes between 300 μm and 1200 μm satisfy these criteria while avoiding phenomena such as early pore occlusion due to very small pores [166] or poor tissue formation and mineralization due to very large pores [170]. A pore size should not be smaller than 100 μm, otherwise, it cannot allow the penetration of thick mineralized tissue other than thin fibrous tissue, and very small pores are of comparable size to cells (10s μm) and hence hinder cell migration [171].

Lattice topologies where struts form acute angles (i.e., triangulated pores) have been found to accelerate cell differentiation compared to topologies with obtuse-angled or circular-shaped pores [166, 172, 173]. While studies in channels of different shapes report that small radius of curvature and the presence of concavities greatly accelerate tissue growth [174, 175]. This is typically attributed to the curvature-driven tissue formation, where tissue preferably grows in concave regions of 3D environments like pore corners [174]. The corners, where struts or sheets meet, are areas of maximum curvature where stresses concentrate. Cells and tissue in these regions experience increased surface tension due to the high curvature; new ECM is formed to bridge the corners and increase the radius of curvature [176]. Cells lying

along the strut length where the curvature is zero are stimulated when their neighbourhood becomes curved due to tissue growing outward from the corners, as more cells sense and bind to the ECM the pores are progressively occluded [177]. Cell proliferation and differentiation are driven by local forces that cells sense from substrate geometry, while smaller pores typically accelerate the rate of tissue formation [178, 179]. Thus, scaffold design has always focused on tuning pore size and geometry to provide physical cues for beneficial cell motility and communication [180, 181].

Stochastic structures more closely resemble the random micro-architecture of trabecular bone and have been shown to promote cellular behavior more effectively than periodic lattices of similar pore size or surface area [81, 167, 182]. Nevertheless, limited data exist on how the topological characteristics of stochastic lattices influence osteogenesis, and most studies have primarily focused on pore size [182, 183]. In such heterogeneous structures, however, pore size typically varies more than in periodic structures, which exhibit a more confined distribution. Therefore, pore size alone may not be sufficient to control cellular behavior in stochastic designs. Most stochastic lattices are designed with an average strut connectivity close to 4, aligning with that of natural trabecular bone (3 to 5 trabeculae per node) [184]. An in vitro study on the effect of topology in stochastic lattices demonstrated that structures with higher strut connectivity promote tissue formation, mineralization, and osteogenic differentiation. This was attributed to the presence of multiple concavities around the nodes and an increased surface area, which facilitates cell communication [129]. These findings suggest that topological modification in stochastic architectures can regulate cell fate, in analogy to periodic structures.

These conclusions are largely based on in vitro experiments in which researchers evaluate cell activities (adhesion, proliferation, and differentiation) through protein expression profiles and mineral deposition over periods of a few weeks. In vivo pre-clinical models, however, provide a more reliable indication of an implant's performance. Several studies have compared AM lattice-based scaffolds with varying porosities, pore sizes, strut thicknesses, and topologies for their ability to promote healing of bone defects of different sizes (representative examples are summarized in Table 2). Most studies rely on micro-CT scanning to quantify total bone ingrowth (i.e., the ratio of newly formed bone volume to the total defect volume) or on mechanical pull-out tests to assess the strength of the bone–implant interface.

Across a wide range of scaffold designs, a pore size of approximately 500–600 μm appears to favour osseointegration regardless of topology. Thinner struts generally promote greater bone ingrowth for a given pore size and topology. However, both in vivo and ex vivo studies [185, 186] indicate that these differences are modest; therefore, strut thickness should be optimized primarily for manufacturability and mechanical performance.

A major limitation of most pre-clinical investigations is the lack of detailed assessment of the quality and maturation state of the bone matrix formed within the porous structures. Distinguishing between early woven bone and more mature lamellar bone, tracking the progression of mineral deposition, and characterizing the matrix at the bone–implant interface require more comprehensive analyses. Complementary histological techniques and fluorochrome labelling approaches should be integrated into future studies to address these gaps [187, 188] and to enable a more rigorous correlation between osseointegration, scaffold design parameters (e.g., porosity, pore size, topology), and the overall size of the implant or defect.

5 | Additive Manufacturing of Lattice Structures

5.1 | Overview of AM Methods

Additive manufacturing has enabled the fabrication of implants with precise dimensions, complex geometries, and great reproducibility, at a cost that is competitive and reducing [193]. For many applications, the final product can be produced with fewer intermediate stages, reduced shipping costs, minimum human intervention, and in less time compared to conventional methods [194]. However, there are disadvantages too: machines are expensive, and a relatively poor surface finish can compromise mechanical performance and dimensional accuracy. Thus, some degree of post-processing (section 6), whether mechanical, laser-based or chemical post-processing, is usually required, increasing manufacturing cost [195].

According to international standards ISO 17296-2 and ASTM 52900 [196, 197], AM processes are formally classified into seven categories (Figure 4): Directed Energy Deposition (DED), Vat Photopolymerization (VPP), Material Jetting (MJT), Binder Jetting (BJT), Material Extrusion (MEX), Powder Bed Fusion (PBF), Sheet Lamination (SL). These classifications encompass the breadth of available feedstocks – including polymers, photopolymers, polymer–ceramic composites, ceramics, and metals – and reflect substantial variation in processing principles, achievable resolution, and material compatibility. A comparative summary of these processes, including typical materials, manufacturing resolution, and the principal advantages and limitations, is provided in Table 3.

Powder bed fusion (PBF) remains the most widely adopted AM class in industrial applications, largely due to its high dimensional precision (10s of μm) and its versatile material selection, which are particularly relevant to orthopedics (e.g., titanium, stainless steel, cobalt-chrome alloys). PBF processes employ a concentrated energy source (laser or electron beam) to selectively fuse regions of a powder bed. The extent of fusion depends on the material system: metallic powders are generally fully melted to create dense components, whereas polymeric and ceramic feedstocks are often partially melted or sintered. This functional distinction has led to widely used commercial subterminology: Selective Laser Melting (SLM) for metals, Selective Laser Sintering (SLS) for polymer or ceramic sintering, and Electron Beam Melting (EBM), where an electron beam is applied predominantly for metals.

5.2 | A Deeper Look at Powder Bed Fusion

Powder bed fusion has emerged as the predominant additive manufacturing method currently used in the orthopedic industry, particularly due to its successful adaptation to key engineering materials such as titanium and its alloys. Its high resolution,

TABLE 2 | Summary of in vivo studies evaluating strut-based lattice implants with varying porosities, pore sizes, and topologies in bone defects.

Topology	Porosity[a]	Pore size[a] (μm)	Strut thickness (μm)	Scaffold dimensions (mm)	In vivo model	Duration of study	Bone ingrowth	Refs.
Diamond	68%	400	315	⌀4 × 6	Femoral condyle of rabbits	12 weeks	12%	[189]
		650	465				21%	
		850	582				17%	
		1100	730				15%	
Octehedral	60%	500	~350	⌀3 × 4	Femoral condyle of rats	12 weeks	23%	[190]
	60%	600					21%	
	60%	700					13%	
	70%	500					23%	
	70%	600					23%	
	70%	700					19%	
Diamond	72%	800	300	⌀5 × 10	Tibial condyle of rabbits	12 weeks	25%	[182]
Stochastic	79%	900					33%	
	83%	1000					38%	
	87%	800					30%	
	91%	900					41%	
	93%	1000					45%	
Octet-truss	60%	N/A	210	⌀16 × 15	Femoral condyle of sheep	6 weeks	7%	[187]
Stochastic	80%	830					9%	
Cubic	40%	700	870	⌀2 × 4	femoral condyle of rats	4 weeks	2%	[191]
	70%	700	360				12%	
	90%	700	210				14%	
	70%	400	210				1%	
	70%	900	450				5%	
Stochastic	60%	500	300	⌀2 × 4	Femoral condyle of rabbits	16 weeks	8%	[192]
	70%	800					20%	
	80%	1000					14%	

[a]Reported values represent as-designed porosity and pore size; corresponding as-built values may differ. "N/A" denotes information not reported.

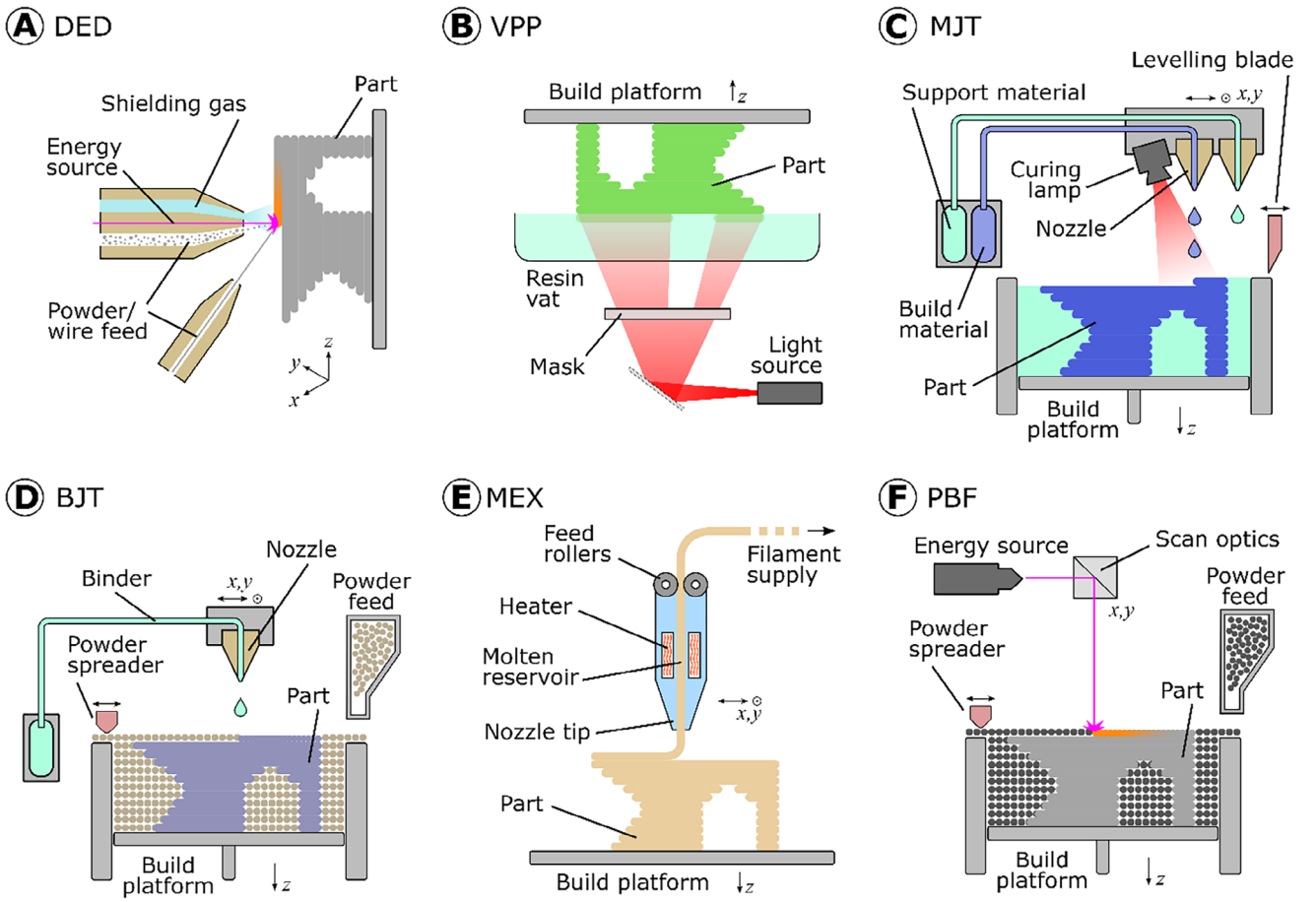

FIGURE 4 | Schematic diagrams of several types of additive manufacturing, showing (A) directed energy deposition, (B) vat photo-polymerisation, (C) material jetting, (D) binder jetting, (E) material extrusion, and (F) powder bed fusion.

design flexibility, and ability to produce complex porous geometries make it especially suitable for creating lattice structures tailored for cementless joint replacement implants. As the field advances, increasing attention has been devoted to optimizing process parameters to ensure dimensional accuracy and eliminate the generation of defects that can compromise mechanical performance.

5.2.1 | Process Limitations

While highly accurate compared to other additive manufacturing methods, powder bed fusion is known to lead to defects affecting the quality and performance of the final products. Major defects include:

- Internal porosity (Figure 5a), often caused by insufficient laser energy leading to incomplete melting of powder particles, or conversely, very high laser energy leading to melt pool turbulence and spatter, leading to entrapped gas (keyhole pores) or lack-of-fusion pores [201].
- Incomplete fusion, where an inadequate energy input or improper scanning strategy results in partially melted regions, compromising the mechanical integrity [202].
- Surface roughness (Figure 5b), manifested as semi-sintered particles due to overheating or even splashing of molten powder, stair-stepping (i.e., visible ridges formed on the edges of 3D objects due to the layer-by-layer printing process's inability to accurately represent sloped or curved geometries), and waviness (due to overlapping melt-pools generated by the laser when binding the powder) [203].
- Residual stresses and warping, usually a product of thermal gradients and rapid solidification, where the differential thermal contraction induces tensile and compressive internal stresses that can cause cracks or part distortion [204, 205].

Computational models incorporating micro-CT data of AM lattice coupons have demonstrated that defects such as waviness and strut/sheet thickness deviations can substantially influence the effective mechanical properties and overall macroscopic deformation response of both strut-based [206] and sheet-based [207] structures. These findings highlight the importance of understanding the source of manufacturing defects and developing predictive models that explicitly account for the probability and spatial distribution of defect occurrence, enabling more accurate assessments of mechanical performance at the design stage.

These defects arise from diverse factors like the energy density and melt-pool dynamics (i.e., size, shape, temperature gradient,

TABLE 3 | Overview of major additive manufacturing methods.

Process	Established Compatible Materials	Typical order of resolution[a] (µm)	Advantages	Disadvantages
Directed Energy Deposition (DED)	Metals Metal-Ceramic Composites	100–1000	Repair or add features to existing parts; High deposition rates; Strong layer bonding	Low resolution; Residual stress; Limited geometric freedom; Poor surface finish
Vat Photopolymerization (VPP)	Photopolymers Polymer-Ceramic Composites	10–100 < 1 for 2-pp	Suitable for complex geometries; Fine feature resolution; Smooth surface finish	Limited to photosensitive resins; Material shrinkage; Essential post-processing (curing)
Material Jetting (MJT)	Photopolymers Elastomers Multiphase polymers	10	Suitable for complex geometries; Smooth surface finish; Multi-material capability	High material and equipment cost; Limited mechanical strength
Sheet Lamination (SL)	Polymers Reinforced Polymer Composites Metals	100	High build speed; Embedding of sensors or electronics	Limited geometry complexity; Weak interlayer bonding; May require adhesive layers
Binder Jetting (BJT)	Metals Ceramics	10–100	Suitable for complex geometries; Low thermal distortion	Material shrinkage; High internal porosity; Requires binder material
Material Extrusion (MEX)	Thermoplastics Reinforced Polymer Composites Biomaterials (i.e., bioprinting)	100	Low cost; Wide material availability; Suitable for biofabrication	Limited feature resolution; Anisotropy due to filament deposition; Surface roughness and porosity
Powder Bed Fusion (PBF)	Metals Polymers Ceramics	10–100	Suitable for complex geometries; High final part density	Possible warping, residual stresses, and anisotropy due to thermal gradients; High equipment and operational cost

[a]Resolution is reported as an order-of-magnitude estimate and may reflect minimum feature size, voxel/pixel dimension, or layer thickness depending on the AM process. Actual achievable resolution varies with machine settings, feedstock characteristics, and post-processing. Data compiled from [198–200].

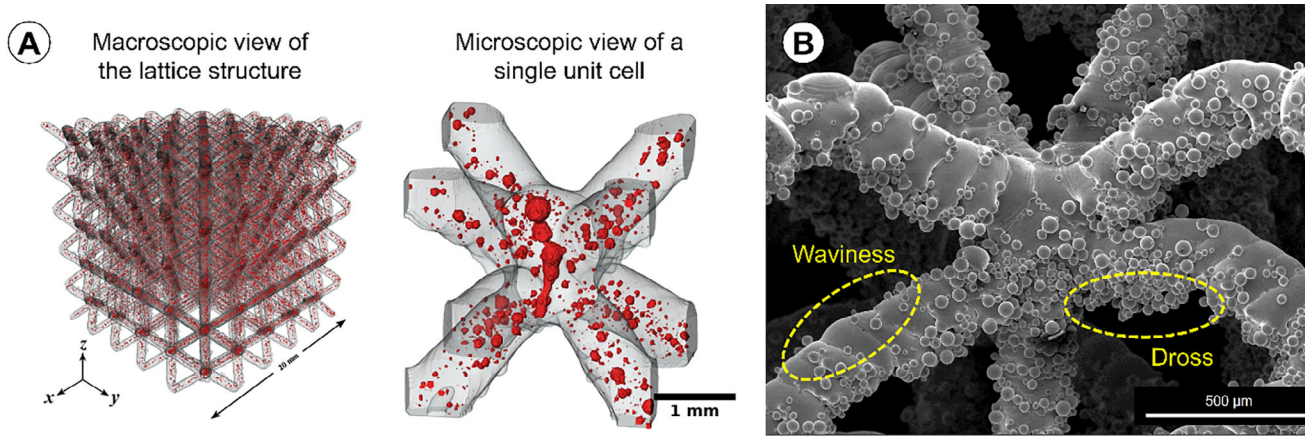

FIGURE 5 | Major defects and limitations in powder bed fusion. (A) Example of entrapped porosity in a periodic lattice structure fabricated using SLM and AlSi10 Mg powder. Micro-CT scanning enabled the visualisation of enclosed pores throughout the lattice structure (macroscopic view) as well as at individual unit cells (microscopic view). Red marks indicate pores. Reproduced with permission [208]. Copyright 2018, Elsevier. (B) Typical forms of surface roughness in a stochastic lattice structure made using SLM and CP-Ti powder. Yellow circles indicate waviness on the upper surface of the struts due to consecutive layer build or dross formed by accumulated semi-sintered particles at the downward-facing surfaces due to overheating. Reproduced with permission according to CC BY 4.0 [129]. Copyright 2023, Frontiers Media.

mass flow, and stability), the layer thickness, the adequacy of supports, powder particle size, and material properties. Among these, energy density and melt-pool dynamics are closely linked to laser parameters such as power, scanning speed, and laser pulse duration. Extensive research on laser parameter optimization has significantly reduced traditional defects like porosity and incomplete fusion in widely used materials such as Ti-6Al-4V and 316L stainless steel.

Particularly in metals, the resulting microstructure and mechanical anisotropy remain persistent challenges during powder bed fusion. The rapid heating and cooling cycles (cooling rate $\approx 10^6$ K/s) lead to thermal gradients and non-equilibrium solidification [209]. The resulting microstructure depends on the thermal gradient and solidification rate and can be planar, cellular, and dendritic [210]. In powder bed fusion, the thermal gradient is $\approx 10^7$ K/m, and the solidification rate is ≈ 0.1 m/s, which, together with the high scanning speed, form an elongated but shallow melt pool. Guided by the shape of the melt pool, the solidified microstructure displays a fine columnar grain structure that aligns with the build direction (Z-axis) [211]. Eventually, this results in anisotropic properties, where the mechanical strength and ductility vary depending on the orientation relative to the build direction. Generally, AM (solid) parts that are built horizontally tend to have higher tensile/compressive strength under quasi-static and fatigue loading compared to vertically orientated parts [212].

The combined effects of structural defects and anisotropy are particularly evident in lattice structures. Their high surface area-to-volume ratio leads to greater defect accumulation than in bulk parts. The mechanical properties of lattice structural elements (i.e., struts) often show trends that contradict those observed in bulk AM parts. Vertically built struts typically exhibit higher strength and elastic modulus, but lower ductility compared to horizontal struts for a variety of materials such as CP-Ti [213], Ti-6Al-4V [214], steel 316L [215], and Al-Si-10Mg [216]. This contradiction between the behavior of fine struts and bulk parts can be explained by the amplified influence of defects generated in low-angled struts.

Vertical struts are built on top of solidified areas from previous layers, which provide heat-conductive routes. On the contrary, low-angled struts are built partially on solid and powder regions, resulting in slower heat dissipation [80]. This slower cooling leads to overheating in the vicinity of low-angled struts, causing high surface roughness in the form of semi-sintered particles and dross at downward-facing surfaces of overhanging struts [217, 218]. Additionally, low-angled struts are more prone to the stair-stepping effect, which can result in poor overlap between consecutive melt-pools and imperfect layer bonding, compromising mechanical strength. Last, vertical struts, being directly aligned with the build direction, may experience more uniform cooling, leading to finer microstructures [219]. Finer grains or more uniform microstructures can increase strength but reduce ductility, making the material more brittle. Overall, the sensitivity of AM struts to defects is also associated with their inferior strength and elastic modulus compared to their respective base (wrought) material, as seen in cases of Ti-6Al-4V and 316L [215, 220].

Last, a major drawback in reproducibility in powder bed fusion systems concerns powder feedstock. Reusing powder for new builds is a common practice. However, it can greatly compromise the dimensional accuracy and the mechanical performance of AM parts. Reused powder exhibits roughened particle surface, aggregations where small (satellite) particles bind to larger ones, and often chemical contamination (impurities and oxidation) [221]. These issues can reduce powder flowability and chemical purity, ultimately leading to higher surface roughness and inferior mechanical properties when AM parts are made using reused powder compared to those made using virgin powder. The effect of powder reuse has also been seen in lattice structures, where lower static/fatigue strength and elastic modulus were recorded for increasing powder reusing cycles, in cases of tantalum [222] and CP-Ti [223].

5.2.2 | Comparison of Powder Bed Fusion Systems

Key differences are found between the two types of metal powder bed fusion systems: SLM and EBM. SLM generally offers higher resolution and finer detail due to the laser's smaller spot size (10 vs. 100 s μm) [224]. However, the high energy density of the laser greatly increases the surface roughness of SLM parts compared to EBM parts. By evaluating the surface quality of commercially available acetabular cups, Nicum et al. found ≈8 times more semi-sintered particles/mm^2 on implants built using SLM compared to EBM, however, the exact combination of process parameters used was not provided in the study [225]. Another major challenge in powder bed fusion is the need for a controlled environment that will minimise the introduction of impurities in the fabricated parts. During SLM, the build chamber is filled with an inert gas, such as argon or nitrogen, which prevents the powder bed from chemically reacting (e.g., oxidation) with the environment. On the contrary, EBM operates in a vacuum and involves a preheating step that reduces thermal gradients and the material solidification rate compared to SLM. This generally results in lower residual stresses and fewer defects like warping.

The high differences in cooling rates (typically 10^4–10^6 K/s in SLM and 10^3–10^5 K/s in EBM) also result in SLM parts exhibiting finer microstructures, which can have contradictory performance under quasi-static or cyclic loading [226]. In a study by Rafi et al. [227], solid Ti-6Al-4V specimens were fabricated through SLM and EBM, and the SLM parts exhibited a martensitic microstructure, resulting in 30% higher tensile strength but 50% less ductility than the EBM parts with lamellar grain morphology. Another example is found in the study of Liu et al. [228], where the same lattice structure was found to have ×10 times more entrapped pores when fabricated using SLM than using EBM. This had a limited effect on quasi-static and high-cycle fatigue strength (low-stress levels), but greatly reduced low-cycle fatigue life (high-stress levels).

Overall, each method exhibits advantages and disadvantages, and choosing between them is primarily a matter of the material being used and design requirements. For example, EBM allows the processing of very brittle metals that would be prone to cracks due to the fast solidification of SLM. At the same time, it poses a limitation on material selection, as not all metals can withstand the vacuum due to sublimation and degradation, especially when containing constituents such as Zn, Mg, and Pb [226].

5.2.3 | Process Control in Laser Powder Bed Fusion

Like most AM processes, PBF begins with the creation of a digital 3D model using a CAD software. The 3D model is then sliced into horizontal layers, producing 2D imprints (i.e., the contour) based on part's height (in respect to the building bed) and layer thickess. Building occurs along the Z-axis, while the slicing software allows the positioning of the part in the X-Y plane, the generation of support structures for overhangs, and the assignment of process parameters. During laser PBF, a firing laser typically hatches the contour of each layer to produce the final 3D part (Figure 6a). The key parameters employed during laser powder bed fusion include the following (Figure 6b):

- Laser power (10s to 100s W),
- Layer thickness (10s of μm),
- Hatching spacing (10s of μm),
- Distance between consecutive exposure points (10s of μm),
- Exposure time of laser (10s to 100s of μs).

Analytical expressions for the energy transmitted to the powder bed are typically used to select process parameters for balancing printing outcome and productivity. The volumetric energy density [J/mm^3] is the most widespread physical entity used in powder bed fusion:

$$ED = \frac{P}{v \cdot h \cdot l} \tag{6}$$

The expression combines laser power P, scan speed v (from one to thousands of mm/s), hatch spacing h and layer thickness l. In case of a continuous laser beam, the scan speed is a fixed value, while for a pulsed laser, it can be assumed equal to:

$$v = \delta_p / \delta_t \tag{7}$$

where, δ_p being firing point distance and δ_t being the laser exposure time.

A limitation of this expression is that it provides a magnitude of energy used without incorporating material-specific information. However, material properties like thermal conductivity and coefficient of thermal expansion affect the precision, surface finish, and potential for defects like warping. Thus, a more accurate physical model should correlate process parameters and material properties to provide insights into the printing process.

An alternative expression defines specific enthalpy delivered to the powder bed ΔH [J/kg] [80, 229] which incorporates laser power P, laser spot diameter Φ (10s of μm), scan speed v, as well as powder material properties (density ρ, absorptivity A, thermal diffusivity D):

$$\Delta H = \frac{A \cdot P}{\rho \sqrt{\pi D v \Phi^3}} \tag{8}$$

This expression on the other hand does not include the layer thickness and hatch spacing, meaning that individual models should be used for different values of the above parameters. Still, it has been shown that melt pool size – which depends on material, power, scanning speed, layer thickness and hatch spacing collectively – affects the internal porosity due to lack of fusion [230, 231]. In this regard, optimizing the powder bed fusion process while keeping layer thickness and hatch spacing fixed appears the most efficient approach. This makes the selection of an appropriate combination of power and scanning speed a central aim for successful printing with low surface roughness and entrapped porosity, parameters which are known to critically affect the mechanical performance of an AM part, particularly the high-cycle fatigue strength [232]. As a general rule, combining high power with low scanning speed leads to increased enthalpy and a large melt pool that, in extreme values, will cause melt

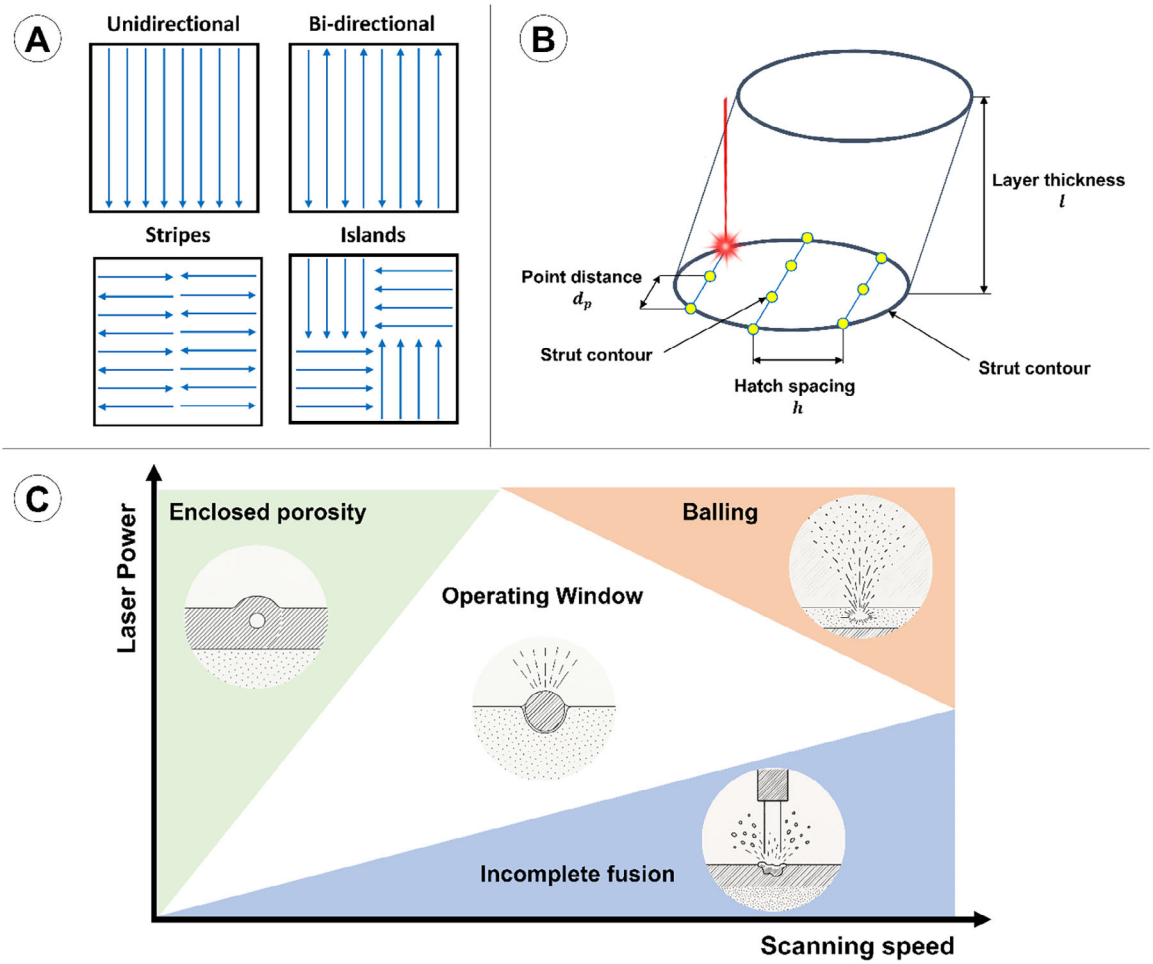

FIGURE 6 | Overview of key aspects influencing part quality in powder bed fusion. (A) Representative scanning strategies for contour filling per layer, illustrating common path planning approaches. (B) Schematic of major process parameters. (C) Process map of laser power versus scanning speed, highlighting regions associated with key defects (e.g., lack of fusion, balling, enclosed porosity), with a central "operating window" indicating optimal process stability.

pool turbulence, powder evaporation and denudation zones. On the other hand, low power and high scanning speed lead to lower enthalpy and smaller melt pool, generating insufficient heat for complete melting and poor overlap between consecutive melt pools. A moderate range of power and scanning speed will enable sufficient melting and a stable melt pool for creating parts with minimal internal porosity and surface defects. This range of optimal parameters can be termed as "operating window" (Figure 6c), with the exact values being dependent on the specific AM system and powder material [229, 233–235].

While these trends were initially observed in bulk AM parts, similar behaviors have been identified in lattice structures. High laser power enables the fabrication of large strut thickness but often introduces a higher percentage of entrapped pores [80, 236]. Increasing laser scanning speed will generally lead to a smaller strut thickness. Interestingly, however, intermediate speeds (4000 mm/s) were found to exhibit higher internal porosity compared to low (1000 mm/s) or high (7000 mm/s) speeds [236]. Hence, a combination of low power and low speed, in conjunction with selected layer thickness and hatch spacing, should produce fine struts with minimal porosity and sufficient melt-pool overlap to ensure structural integrity.

5.2.4 | Recent Advancements in Powder Bed Fusion Systems

The fabrication of complex structures using established materials such as Ti-6Al-4V, 316L, and Al-Si-10Mg is now well documented and understood. Current research efforts aim at introducing new materials for lattice-based implants, such as magnesium alloys with tailored degradation rates [237], and multi-material additive manufacturing that enables spatially varied mechanical and biological properties [238, 239].

Despite significant progress, challenges such as anisotropic mechanical behavior and residual stresses persist. To address these issues and enhance industrial scalability, recent advancements include adaptive layer thickness for reduced surface roughness [240], multi-laser and beam-shaping technologies for increased productivity and uniform melting [241], real-time in situ monitoring combined with AI-driven adaptive control for defect mitigation and quality assurance [242, 243], and digital twin frameworks for process simulation and optimization [244]. Together, these innovations are transforming PBF from a prototyping tool into a robust, regulated production route for orthopaedic implants.

6 | Post-Processing Methods for AM Lattice Structures

6.1 | Post-Processing for Mechanical Performance

Defects such as semi-sintered particles, residual stresses, internal porosity, and microstructural heterogeneity are particularly harmful to fatigue strength as they can lead to stress concentrations and become crack initiation sites during cyclic loading [140, 245]. Post-processing treatments are utilised to rectify such defects and ameliorate the mechanical performance of additively manufactured parts.

The most widely used post-processing treatments for powder bed fusion parts concern surface and heat treatments. Surface treatments aim at enhancing the surface finish with or without material removal, and they comprise mechanical methods (e.g., machining, media blasting, vibratory finishing), chemical methods (e.g., chemical etching, electropolishing), and laser-based methods (e.g., laser micro-machining, laser shock peening) [195]. In contrast, thermal treatments are applied to release any residual stresses or to induce microstructure changes within a part.

6.1.1 | Surface Treatments

Media blasting (e.g., sandblasting) and vibratory finishing are the most common mechanical methods to smooth the surface of additively manufactured specimens. However, in the case of lattice structures, the abrasive media used in such methods cannot typically reach the core of the specimens owing to the complex porous architecture. The same limitation occurs also in the case of laser-based methods where the laser cannot reach regions in the core of the part. Hence, chemical-based methods are more suitable for surface finishing of AM lattice structures.

Chemical etching is the most widely used surface treatment applied in lattice structures (Figure 7c,d). A chemical reagent reacts with the AM substrate, leading to material removal through controlled corrosion. Typical reagents constitute strong and highly corrosive acids like nitric acid, sulfuric acid, and hydrochloric acid. Since they rely on a fluid media, chemical etching has been successfully used to remove semi-sintered particles from lattice structures. This process reduces the surface irregularities and stress concentration sites, however it often introduces pits on the surface due to the removal of the semi-sintered particles [246]. More importantly, chemical etching is inevitably accompanied by a reduction in strut/sheet thickness and eventually in relative density, which becomes more apparent for prolonged times of etching [247, 248]. Lower relative density results in drastically reduced static and fatigue strength. Thus, the absolute S-N curves in fatigue testing of the initial (as-built) specimens appear higher than the chemically etched specimens. If normalised stress values are used, the superior fatigue performance of chemically etched specimens is evident. This has been previously shown in lattices made with Ti-6Al-4V [249] and CoCr [246, 250]. This is attributed to the significantly higher tensile strength of etched struts compared to as-built struts. For the same apparent strut diameter, a larger portion of the strut can effectively carry a load in etched than in as-built struts, owing to lower waviness and semi-sintered particles that do not contribute to the strength [251].

Although a well-established surface treatment, conventional chemical etching relies on immersing the parts in the acid solution. This introduces limitations when using large-sized lattice structures, as the acid cannot penetrate deeply or evenly inside the lattice [252]. This leads to uneven etching, with the material removal being more aggressive at the outer regions and less effective near the core of the lattice. Applying a fluid flow in the etchant is also avoided as it can induce even higher heterogeneities in the material removal.

To address these challenges, hybrid chemical–electrochemical surface treatments have been developed to combine hydrodynamic flow and electrolytes capable of removing large-scale roughness (10–100s of μm) that typically cannot be removed with conventional electropolishing [195]. Such methods have successfully applied to Ti-6Al-4V lattice structures, resulting in an 80% increase in normalised fatigue strength compared to untreated structures [253] (Figure 7g-i).

6.1.2 | Thermal Treatments

Heating for stress relief in the case of lattice structures is more relevant when they are combined with solid sections within the same component. Solid parts are more prone to wrapping or cracking owing to residual stresses. In contrast, lattice structures do not experience such substantial residual stresses since struts are unconfined and free to deform during the manufacturing process [254].

High-temperature annealing is traditionally employed for alloyed metals to induce more ductile behavior. Some representative examples are found in the case of Ti-6Al-4V. Yuan et al. evaluated meshes that were annealed at sub-transus temperatures: 750°C, 850°C, and 950°C to transform the as-built martensite α-phase to coarse lamellae, which improved structures' ductility, and eventually fatigue life [255]. While Ghouse et al. compared the fatigue strength of stochastic lattices subjected to sub-transus (920°C) and super-transus (1050°C and 1200°C) heat treatments, below and above the β-transus temperature [106]. Sub-transus heat treatments improved the fatigue strength by 59% compared to the as-built condition due to the replacement of brittle α' martensite with the equilibrium α phase. Super-transus heat treatment was expected to be less effective due to recrystallisation of coarse-grained β, however resulted in an even larger 75% increase in fatigue strength (Figure 7f). This was attributed to additional sintering of semi-fused particles, highlighting how heat treatment methods developed for conventional forged components must be modified for lattice structures.

Hot-isostatic pressing (HIP) provides a combination of increased ductility due to the generation of coarser grains and an increase in specimen density due to the closure of pores [254] (Figure 7a,b). Numerous studies have shown that HIP, especially when combined with chemical etching, significantly increases the fatigue

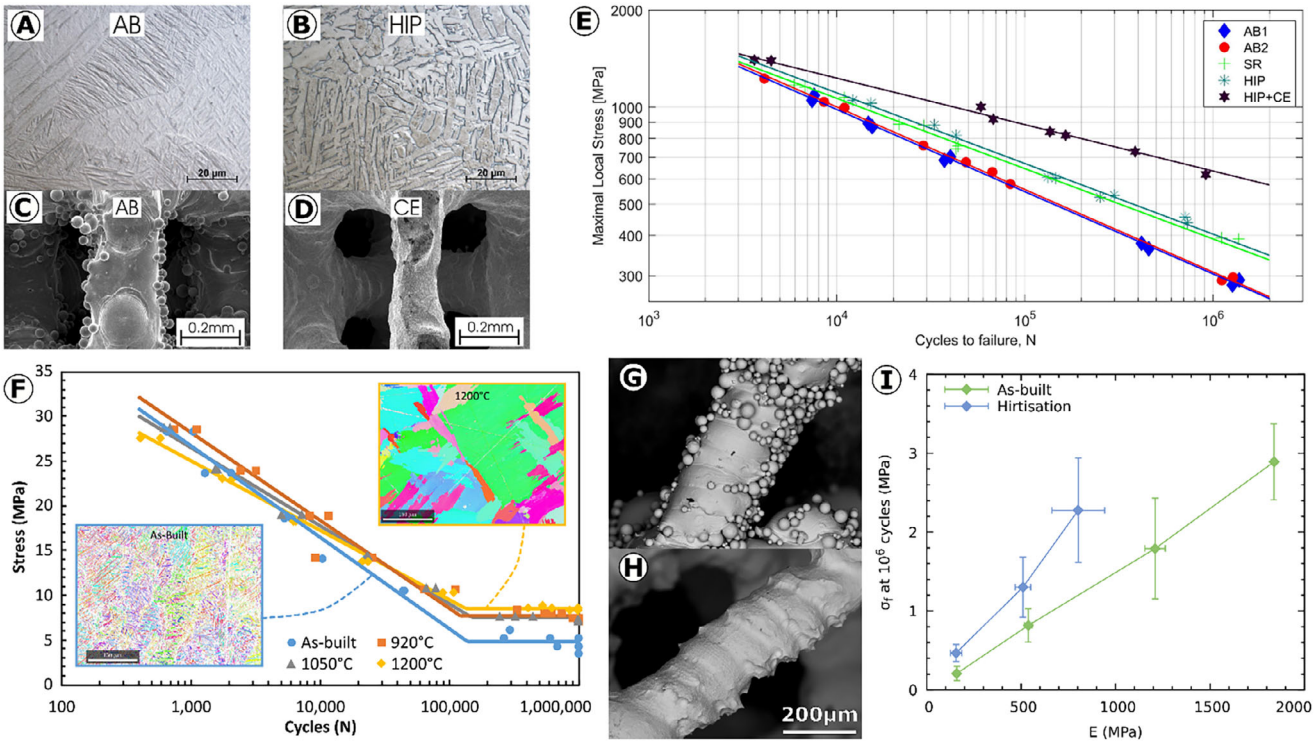

FIGURE 7 | Effects of post-processing techniques on fatigue behavior of Ti6Al4V. (a–e) Reproduced with permission [249]. 2017, Copyright Elsevier. (a–d) show the microstructures of as-built (AB) and hot isostatically pressed (HIP) Ti6Al4V, and SEM images of strut surfaces in AB and CE (chemically etched) conditions. (e) shows the effect of these treatments on the fatigue behavior. (f) Shows the effect of vacuum heat treatment on microstructure (electron back-scatter diffraction maps inset) and the resulting fatigue behavior. Reproduced with permission according to CC BY 4.0 [106]. Copyright 2021, Elsevier. (g–i) show SEM images of strut surfaces before (g) and after (h) chemical–electrochemical surface treatment. (i) shows the ultimate fatigue strength vs. modulus for the AB condition and after chemical–electrochemical surface treatment, demonstrating improved fatigue performance for a particular target modulus. (g–i) Reproduced with permission according to CC BY 4.0 [253]. Copyright 2023, Elsevier.

strength of lattices [246, 249, 256]. However, optimizing grain size remains an active area of research, especially with the continual development of new alloys for additive manufacturing. Therefore, a sequential approach combining heat treatment, surface treatment, and HIP offers a promising strategy to tailor microstructure and correct manufacturing defects, ultimately maximising mechanical performance (Figure 7e).

6.2 | Post-processing for Osteoconductivity

Grafts for bone regeneration should combine two major biological characteristics: osteoconduction and osteoinduction. Osteoconduction refers to the ability of the material to support cell adhesion, proliferation, matrix formation, and ultimately, mature bone formation [16]. Osteoinduction refers to the ability of a material to induce bone formation when implanted even at sites where bone is not normally found (heterotopic sites) [257]. Of these two, osteoconduction is more relevant in the context of cementless implants for joint replacement.

Post-processing techniques can be applied to introduce bioactivity in implants, encompassing physical methods, chemical methods, and biomimetic coatings. In most cases, these methods aim at activating the implant surface to exhibit chemical reactivity or physical characteristics that benefit cell function.

6.2.1 | Physical Methods

Key examples of physical post-processing methods are media blasting, polishing, laser engraving, plasma treatment, and heat treatment.

The first two mechanical treatments aim to introduce micro-scale roughness that benefits osteoblast adhesion, proliferation, and differentiation. This is investigated using the surface roughness parameters Ra (average roughness) and Rz (average maximum height of the profile). Ra values around 1–2 µm [258–260] and Rz values between 1 and 10 µm [261] have been shown to favor cell adhesion and protein adsorption due to the high surface area and wettability, and stimulate osteoblastic differentiation due to the introduction of surface discontinuities comparable to cell size (~10 µm).

Nanotexturing achieved through laser engraving is another method to enhance cell adhesion by increasing surface wettability, while also introducing nano-patterns that cells can sense, leading to adjustments in their morphology and orientation toward an elongated shape, which favors differentiation [262, 263].

However, mechanical treatments have two major limitations. First, they can introduce contaminants by leaving residual particles on the implant surface [264]. This issue is particu-

larly associated with sandblasting, leading to its replacement by cleaner alternatives such as dry ice blasting (i.e., carbon dioxide), where no harmful chemicals are used [265]. Second, regardless of the blasting medium, these methods are primarily applied to solid implants, as the complex architecture of 3D lattices does not allow homogeneous treatment throughout the structure.

Plasma treatment and heat treatment are more suitable for lattices, while they have also been extensively used in solid implants in clinical practice [266, 267]. These treatments are typically used in metals like titanium to enhance their bioactivity by creating a thick oxide layer (e.g., titanium dioxide, TiO_2). This oxidation layer demonstrates a nanostructured topography that increases the surface hydrophilicity and thus enhances protein adsorption and cell adhesion [268]. More importantly, it improves the metal's resistance to corrosion, while also enabling reaction with certain dissolved salts [269]. The latter is crucial for the osseointegration of metallic implants as it allows the formation of bone-like apatite (e.g., hydroxyapatite) on the surface of the implant due to the reaction of the oxidised layer with the Ca^{2+} and PO_4^{3-} ions found in body fluids [270].

6.2.2 | Chemical Methods

The application of anodisation and etching with acids or alkaline solutions is also used to enhance the hydrophilicity and bioactivity of metals by creating a nanostructured oxidised layer [271]. Acids and alkaline solutions can improve the chemical reactivity of the surface by removing contaminants and impurities, while in some cases also introducing micro-roughness due to etching [272]. Typical etchants constitute strong acids (e.g., HCl) and strong alkaline solutions (e.g., NaOH), while the combination of chemical and heat treatment has been shown to further enhance implant bioactivity. As a comparison to physical methods, the combination of HCl and heat treatment on titanium implants has been shown to enhance early in vivo bone formation compared to sandblasted or untreated samples [273]. In addition, NaOH-heat-treated implants have been shown to induce stronger bone-implant bonding compared to untreated implants made of pure and alloyed titanium [274]. This is again attributed to the oxidised titanium layer that promotes mineralized bone tissue formation, without the intervention of fibrous tissue typically seen in untreated implants. However, a further improvement in bioactivity has been noted when NaOH-heat-treated implants are further treated with HCl to dissolve the released sodium ions introduced due to the oxidation [275].

Chemical etching (CE) with highly corrosive acids (such as hydrofluoric and sulfuric acid) is often applied to AM lattices to smooth structure surfaces for improved fatigue performance. Previous in vitro experiments have led to unclear conclusions regarding the effect of CE on biological response. Wysocki et al. [252] and Rovetta et al. [276] reported no significant differences in cell proliferation or osteogenic differentiation between etched and as-built AM structures using osteoblast cell lines (e.g., MCT3T3 and MG63). In contrast, O'Keeffe et al. [248] demonstrated that chemical etching enhanced osteogenic differentiation and tissue mineralization in titanium scaffolds seeded with human mesenchymal stem cells. A recent in vivo study in rats by Wang et al. [277] reported higher bone ingrowth and thicker matrix formation in flow-assisted chemically etched titanium scaffolds compared to conventionally CE and as-built scaffolds. These findings highlight the importance of using flow when performing CE for uniform removal of semi-sintered particles across the depth of the porous structures [253]. Moreover, surface smoothing of AM lattices can offer two additional advantages: (i) increased wettability of individual struts, which promotes cell adhesion [276], and (ii) reduced risk of large metallic debris detachment, which could elicit immune responses leading to osteolysis and implant loosening [278].

6.2.3 | Biomimetic Coatings

A final method to increase bioactivity in metallic implants is the application of surface coatings that mimic the environment of the bone matrix.

Hydroxyapatite [$Ca_{10}(PO_4)_6(OH)_2$] and β-tricalcium phosphate [$Ca_3(PO_4)_2$] have been widely used as porous grafts or as a coating in clinical practise for several decades to enhance osseointegration on metallic implants. They can be used separately or combined, and can be applied via plasma spraying, electrodeposition, or sol-gel methods [279–281]. They are typically used in solid press-fit implants that rely on ongrowth, and have been proven to be reliable for promoting mature bone tissue formation compared to untreated implants that are prone to fibrous tissue formation [280]. While in vivo data suggest that these two coatings perform equally [280, 282], synthetic hydroxyapatite is typically considered a permanent rather than degradable implant material, while β-tricalcium phosphate is generally resorbed within a few weeks after implantation [283]. However, a persistent challenge with ceramic coatings is achieving strong and durable adhesion to metallic substrates. Although significant advances have been made in coating technologies, issues such as cracking and delamination can still occur in some cases, potentially leading to localised inflammation due to wear particles [284].

Alternative forms of coatings are the immobilisation of ECM products on metal surfaces. Collagen type-1, which is the primary organic component of bone, can be applied through various methods such as physical adsorption, dip-coating, and covalent bonding and serve as a biomimetic matrix that supports cell adhesion and encourages the formation of new bone tissue around the implant [285, 286]. Glycoproteins such as fibronectin and vitronectin can be applied in similar ways, aiming to enhance osteoblast attachment [287].

Attachment of growth factors on implant surfaces through physical adsorption [288, 289], covalent bonding [290], and encapsulation within carrier materials like hydrogels [291] and nanoparticles [292] has also been investigated. These approaches aim to enhance osseointegration by promoting bone healing and vascularization. However, key challenges include optimizing dosage and controlling the spatiotemporal release of growth factors. Many coatings carry supraphysiological doses and can lead to uncontrolled release, posing risks such as (a) ectopic bone formation, especially in the case of implant misplacement, (b) osteolysis, (c) immunological reactions, and (d) tumorigenesis.

Peptides that mimic specific cell-binding motifs can be chemically grafted or immobilised onto the implant, promoting targeted interactions with cell surface receptors. A typical example is the Arg-Gly-Asp (RGD) sequence, which binds to integrin receptors of cells and aids cell adhesion [293, 294]. The advantage of peptides is that they can be designed to target specific cell surface receptors and promote tailored cell functions. In this context, previous works have shown how different peptides can be grafted on the same implant surface to induce cell adhesion, antimicrobial activity, osteogenesis, and angiogenesis [295–297].

7 | Discussion

7.1 | Current State-of-the Art and Clinical Outcomes

Multiple manufacturers now have a commercially available orthopedic (cementless) implant made using additive manufacturing with integrated lattice sections – typically thin layers (1–2 mm) – at the implant-bone interface to induce osseointegration. This new generation of implants may lead to better long-term fixation in active patients and offer a short-term benefit of reduced operation time. In most cases, commercial AM lattice implants are made of Ti-6Al-4V, tantalum, or CP-Ti, post-processed with heat treatment but without further surface modifications or coatings. They are widely employed in arthroplasty procedures involving the ankle, knee, hip, spine, and shoulder [298] (Figure 8a,b).

The ankle joint often requires implants due to critically sized bone defects or arthritis affecting various regions. Additive manufacturing enables the production of personalised devices, with Abar et al. reporting a 74% success rate in complex cases that had previously failed both operative and non-operative treatments [299]. These implants utilize gyroidal porous structures, which are also applied in foot and ankle wedges. Similarly, Gross et al. demonstrated high success rates with AM ankle replacements, noting significant improvements across all domains of Patient Reported Outcome Measures (PROMs), and a lower revision rate compared to non-AM implants at 6- and 12-month follow-ups [300].

Knee arthroplasty has seen significant advancements in AM implants, enabling cementless devices with enhanced bone ingrowth capabilities. Restrepo et al. demonstrated that total knee replacements featuring a stochastic lattice on the bone-interfacing surface result in long-term bone fixation through bone ingrowth, with a study of 341 implants showing significantly higher survivorship and patient satisfaction ($p < 0.001$) at 4 to 6.8 years follow-up compared to cemented alternatives [301]. Midterm studies (5-6 years) by Fricka et al. and Hannon et al. reported no significant differences in patient satisfaction or radiographic outcomes between cemented and cementless implants [302, 303].

Numerous similar lattice technologies and structures have been effectively applied in acetabular hip cups, consistently demonstrating high success rates for bone ingrowth as evidenced by animal studies – e.g., reports for the OsseoTi by Zimmer Biomet, USA [304]. Berlinberg et al. reported promising clinical outcomes for a fully AM titanium acetabular shell, with 68 patients followed for over two years, revealing an 81% revision-free survivorship rate for all causes [305]. This outcome is particularly noteworthy given the complexity of the cases reviewed. Similarly, Tamaki et al. reported robust results up to 24 months post-surgery, with no cases of aseptic loosening necessitating revision [306].

Spinal fusion cages increasingly incorporate AM lattices to enhance bone ingrowth, utilising similar technologies and characteristics found in knee and hip implants (Restor3D, Stryker). McGilvray et al. compared an AM titanium lattice to a Poly-Ether–Ether–Ketone (PEEK) counterpart, demonstrating significantly greater bone ingrowth at both 8- and 16-weeks post-implantation ($p < 0.01$) [307]. Furthermore, van den Brink and Lamerigts reported complete osseointegration in a two-year postoperative study, indicating that the AM fusion cage facilitated significant bone ingrowth while minimising stress shielding [308]. Donaldson et al. found that 3D-printed scaffold cages exhibited lower subsidence rates than historical fusion cages, with a subsidence rate of only 3.03% in a cohort of fifty patients, followed for a median of 11.3 months [309]. Additionally, Corso et al. reported low early revision rates (6 months) for both PEEK and AM titanium implants, highlighting the reliability and effectiveness of AM technologies in spinal fusion applications [310].

Numerous additively manufactured shoulder implants (glenoid component and humeral stem) are now available, though published clinical data on their effectiveness is still limited due to their recent introduction.

Regarding the lattice characteristics, the majority of commercial implants employ stochastic structures, with periodic structures being less common. The mean pore size of these structures typically ranges between 300 and 650 μm, strut thicknesses range from 230 to 400 μm, and the resulting porosity ranges from 60% to 75% [311–313].

7.2 | Existing Challenges and Direction for Future Research

Optimizing the performance of AM lattice-based implants remains an active area of research across both academia and industry. Successful osseointegration requires careful alignment of mechanical and biological performance to maintain bone health and support regeneration. The rapid evolution of AM technologies has enabled the fabrication of highly complex lattice architectures in a wide range of materials, including metals, polymers, ceramics, and composites. The choice of AM method should be guided primarily by material compatibility, while the selection of lattice type must balance manufacturability with intended biological and mechanical function. Key design parameters, such as porosity, strut or wall thickness, and topology, must be tuned to achieve sufficient fatigue strength for load-bearing applications, bone-matching stiffness to prevent stress shielding and promote active bone remodelling, and spatial cues that can direct cell activity toward maturation and mineralized bone formation.

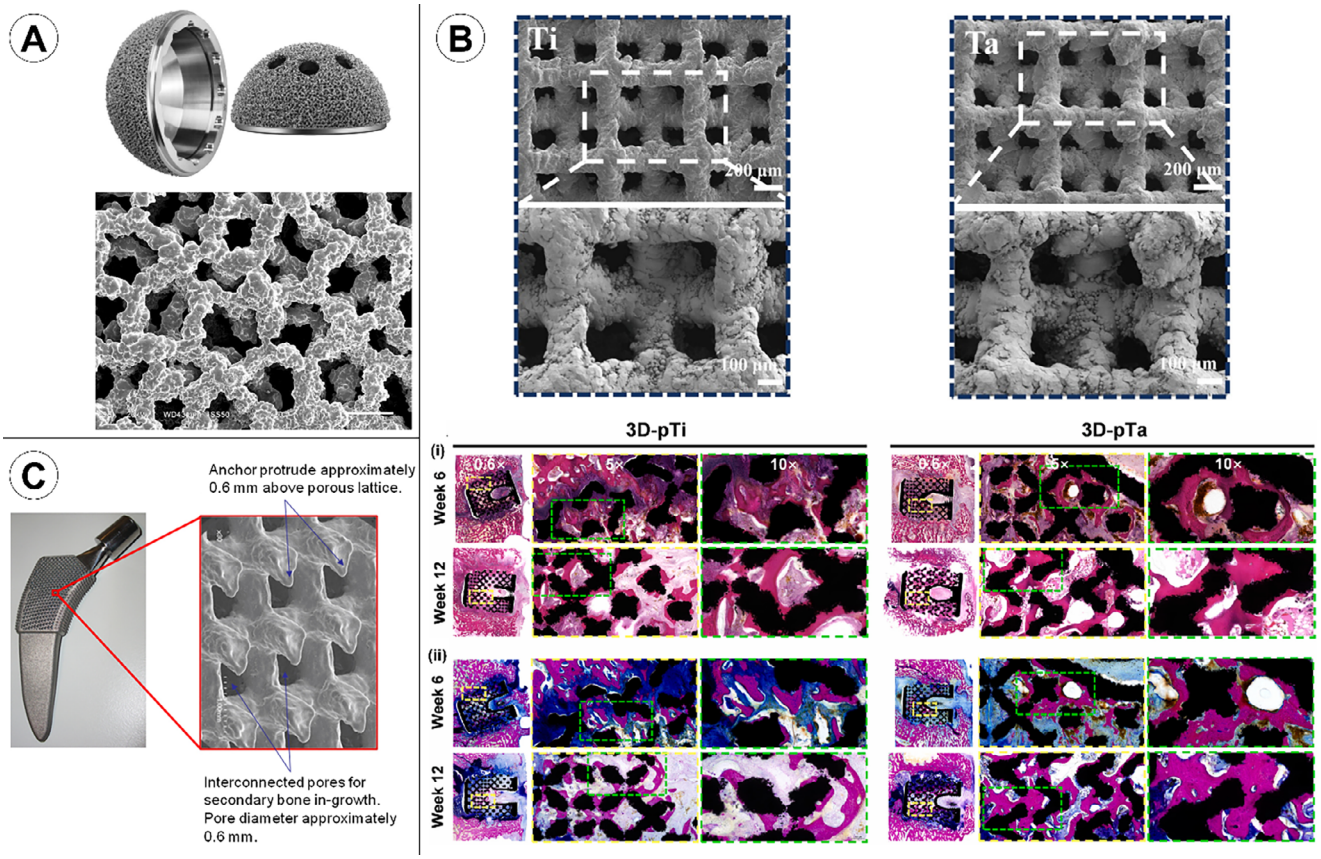

FIGURE 8 | Application of additively manufactured lattice structures in cementless orthopedic implants. A. Acetabular cup made of Ti6Al4V (3D ACT, JRI Orthopaedics, UK). The figure includes a macroscopic photograph of the implant and a scanning electron microscopy (SEM) image of the stochastic lattice micro-architecture. Reproduced with permission according to CC BY 4.0 [327]. Copyright 2020, Springer Nature. B. Spinal cage prototypes made of CP-Ti and tantalum. SEM images show a rhombic dodecahedron lattice structure, along with histological sections after 6 and 12 weeks of implantation in the cadaveric spines of sheep. Histological stains include (i) H&E and (ii) methylene blue–acid fuchsin. Reproduced with permission according to CC BY 4.0 [328]. Copyright 2025, Elsevier. C. Femoral stem made of Ti6Al4V featuring anchoring protrusions at the lattice surface to reduce post-implantation micromotion (OsteoAnchor, Loci Orthopaedics, Ireland). Reproduced with permission [315]. Copyright 2013, Elsevier.

The influence of microarchitecture on osseointegration has been extensively studied in vivo. However, most studies evaluate tissue ingrowth through volumetric filling alone, without assessing collagen fiber orientation or level of mineralization level – both of which are critical determinants of bone quality and functionality. Furthermore, most preclinical evidence is derived from small animal models that do not reflect the biomechanical environment, loading conditions, or metabolic constraints of human bone.

Stabilisation of the implant after surgery is another key factor for tissue formation and maturation. AM provides high design flexibility to develop implants that can reduce implant micromotion. Previous concepts included the incorporation of screw-like [314] or anchoring [315] features for enhanced initial fixation (Figure 8c). More effective modern solutions aim at developing lattice structures with auxetic characteristics that can interlock within the bone [316, 317].

Achieving a low modulus similar to bone using synthetic materials typically compromises mechanical strength. Ensuring high fatigue strength should remain a priority in the development of lattice-based implants. This can be addressed through effective post-processing treatments tailored to the base material, as well as by exploring novel lattice designs. Strategies such as hybrid structures [318, 319], which combine different topologies, and graded structures [320], which integrate varying densities, offer promising solutions to enhance mechanical performance while maintaining the necessary flexibility for long-term implant stability.

Apart from mechanical requirements, the lattice structure should provide topological cues that promote mature bone tissue formation and long-term preservation. Bone is a highly vascularized tissue with significant metabolic demands, so effective angiogenesis and vascularization at the implant site are essential to ensure sufficient oxygen and nutrient supply, preventing cell death and heterogeneous tissue growth [321]. This remains a major challenge, particularly in large porous structures, where early tissue formation at the outer regions can inhibit oxygen supply to the core. Introducing gradient porosity is a promising strategy to coordinate bone tissue formation and vascular infiltration at varying depths within lattice structures. Computational modeling and AI-assisted design can further advance this approach by generating gradient architectures that closely match local bone stiffness while maintaining high permeability for efficient fluid

transport [322]. By incorporating CT-derived data, these methods enable the creation of patient-specific implants that achieve both mechanical compatibility and biological functionality with potential application to joint replacement [323] or bone defects reconstruction [324].

Similarly, bioactive coatings or growth factor delivery systems, such as VEGF-loaded carriers, can enhance angiogenesis in the core regions. More recently, oxygen-generating particles have shown potential in promoting bone formation and vascularization in critical-sized defects when incorporated into hydrogels [325]. Adapting such strategies for lattice structures could support uniform tissue formation throughout the implant by modulating local oxygen availability.

Modifying surface chemistry to enhance osteoconduction and potentially osteoinduction is of particular interest for metallic structures. While these materials are biocompatible, causing minimal toxicity or inflammatory responses, they lack inherent bioactivity compared to bioactive glasses or calcium phosphate ceramics, which exhibit the same chemical composition as natural bone [326]. This underscores the importance of combining effective post-processing and coating strategies to improve bioactivity. However, osteoinductive coatings still face significant challenges regarding long-term stability and controlled release kinetics. Additionally, regulatory approval for novel bioactive coatings remains a major hurdle, necessitating extensive in vivo validation to ensure safety, efficacy, and reproducibility. Addressing these challenges will be crucial for the successful clinical translation of advanced lattice-based implants.

Conflicts of Interest

M.J. Munford and F.C.H. Masure have a financial interest in OSSTEC Ltd. The authors affirm that this review was conducted objectively and is based solely on scientific evidence.

Data Availability Statement

The authors have nothing to report.

References

1. GBD 2021 Osteoarthritis Collaborators, "Global, Regional, and National Burden of Osteoarthritis, 1990–2020 and Projections to 2050: A Systematic Analysis for the Global Burden of Disease Study 2021," *The Lancet Rheumatology* 5 (2023): 508–522.

2. J. B. Driban, M. S. Harkey, S. H. Liu, M. Salzler, and T. E. McAlindon, "Osteoarthritis and Aging: Young Adults with Osteoarthritis," *Current Epidemiology Reports* 7, no. 1 (2020): 9–15.

3. S. Konan, M. P. Abdel, and F. S. Haddad, "Cemented versus uncemented hip implant fixation," *Bone & Joint Research* 8, no. 12 (2019): 604–607.

4. K. F. Hughes, M. D. Ries, and L. A. Pruitt, "Structural Degradation of Acrylic Bone Cements Due to in Vivo and Simulated Aging," *Journal of Biomedical Materials Research Part A* 65A, no. 2 (2003): 126–135.

5. M. Tatullo, M. Marrelli, F. Mastrangelo, and E. Gherlone, "Bone Inflammation, Bone Infection and Dental Implants Failure: Histological and Cytological Aspects Related to Cement Excess," *Journal of Bone and Joint Infection* 2, no. 2 (2017): 84–89.

6. R. Dimitriou, E. Jones, D. McGonagle, and P. V. Giannoudis, "Bone Regeneration: Current Concepts and Future Directions," *BMC Medicine* 9 (2011): 66.

7. M. Stilling, F. Madsen, A. Odgaard, et al., "Superior fixation of pegged trabecular metal over screw-fixed pegged porous titanium fiber mesh," *Acta Orthopaedica* 82, no. 2 (2011): 177–186.

8. S. Bhimji and R. M. Meneghini, "Micromotion of Cementless Tibial Baseplates: Keels with Adjuvant Pegs Offer More Stability than Pegs Alone," *The Journal of Arthroplasty* 29, no. 7 (2014): 1503–1506.

9. D. Downing, B. Lozanovski, T. Williamson, et al., "Fixation Strength of Conformal Additively Manufactured Ti6Al4V Implants in Large Animal Model," *The International Journal of Advanced Manufacturing Technology* 132 (2024): 3977–3992.

10. K. Mustafa, A. Wennerberg, J. Wroblewski, K. Hultenby, B. S. Lopez, and K. Arvidson, "Determining Optimal Surface Roughness of TiO2 Blasted Titanium Implant Material for Attachment, Proliferation and Differentiation of Cells Derived from human Mandibular Alveolar Bone," *Clinical Oral Implants Research* 12, no. 5 (2001): 515–525.

11. S. Vercaigne, J. G. C. Wolke, I. Naert, and J. A. Jansen, "The Effect of Titanium Plasma-sprayed Implants on Trabecular Bone Healing in the Goat," *Biomaterials* 19, no. 11–12 (1998): 1093–1099.

12. J. R. Davey and W. H. Harris, "Loosening of Cobalt Chrome Beads from a Porous-Coated Acetabular Component," *Clinical Orthopaedics and Related Research* 231 (1988): 97–102.

13. J. W. M. Vehof, M. T. U. Haus, A. E. De Ruijter, P. H. M. Spauwen, and J. A. Jansen, "Bone formation in Transforming Growth Factor beta-1-loaded titanium fiber mesh implants," *Clinical Oral Implants Research* 13, no. 1 (2002): 94–102.

14. N. B. Damm, M. M. Morlock, and N. E. Bishop, "Friction Coefficient and Effective Interference at the Implant-bone Interface," *Journal of Biomechanics* 48, no. 12 (2015): 3517–3521.

15. Z. Wang, C. Wang, C. Li, et al., "Analysis of Factors Influencing Bone Ingrowth into Three-dimensional Printed Porous Metal Scaffolds: A Review," *Journal of Alloys and Compounds* 717 (2017): 271–285.

16. T. Albrektsson and C. Johansson, "Osteoinduction, Osteoconduction and Osseointegration," *European Spine Journal* 10 (2001): S96–101.

17. Ł. Łapaj, J. Sulej-Chojnacka, J. Rozwalka, et al., "Debonding of Porous Coating: A Late Failure Mode of Uncemented, Partially Threaded Acetabular Components—Retrieval Analysis," *Journal of Thermal Spray Technology* (2024).

18. P. M. Bonutti, R. Pivec, K. Issa, et al., "Delamination of Tantalum Porous Coating from a TKA Due to Regional Dissemination of Debris," *Orthopedics* 36, no. 8 (2013): 600–604.

19. J. C. Stoddart, A. Garner, M. Tuncer, A. A. Amis, J. Cobb, and R. J. Van Arkel, "Load Transfer in Bone after Partial, Multi-compartmental, and Total Knee Arthroplasty," *Frontiers in Bioengineering and Biotechnology* 12 (2024): 1274496.

20. J. Wolff, "Concept of the Law of Bone Remodelling," (1986): 1.

21. G. H. van Lenthe, W. de M. C. Malefijt, and R. Huiskes, "Stress Shielding after Total Knee Replacement May Cause Bone Resorption in the Distal Femur," *The Journal of Bone and Joint Surgery British volume* 79, no. 1 (1997): 117–122.

22. E. M. Forlenza, J. Serino, E. B. Terhune, M. T. Weintraub, D. Nam, and C. J. Della Valle, "Cementless Total Knee Arthroplasty Is Associated with Early Aseptic Loosening in a Large National Database," *The Journal of Arthroplasty* 38, no. 7 (2023): S215–S220.

23. J. M. Shum, B. C. Gadomski, S. J. Tredinnick, et al., "Enhanced Bone Formation in Locally-optimised, Low-stiffness Additive Manufactured Titanium Implants: An in Silico and in Vivo Tibial Advancement Study," *Acta Biomaterialia* 156 (2023): 202–213.

24. W.-M. Chen, Y. M. Xie, G. Imbalzano, et al., "Lattice Ti Structures with Low Rigidity but Compatible Mechanical Strength: Design of

Implant Materials for Trabecular Bone," *International Journal of Precision Engineering and Manufacturing* 17, no. 6 (2016): 793–799.

25. D. K. Witmer and R. M. Meneghini, "Cementless Total Knee Arthroplasty: Patient Selection and Surgical Techniques to Optimize Outcomes," *Seminars in Arthroplasty* 29, no. 1 (2018): 50–54.

26. L. E. Bayliss, D. Culliford, A. P. Monk, et al., "The Effect of Patient Age at Intervention on Risk of Implant Revision after Total Replacement of the Hip or Knee: A Population-based Cohort Study," *The Lancet* 389, no. 10077 (2017): 1424–1430.

27. M. Weber, T. Renkawitz, F. Voellner, et al., "Revision Surgery in Total Joint Replacement Is Cost-Intensive," *BioMed Research International* 2018 (2018): 1–8.

28. M. B. Schaffler, W. Y. Cheung, R. Majeska, and K. O. Osteocytes, "Master Orchestrators of Bone," Vol. 94 (2014): 5–24. 94.

29. H. M. Frost, *Bone's Mechanostat: A 2003 Update. Anatomical Record – Part A Discoveries in Molecular, Cellular, and Evolutionary Biology*, Vol. 275 (Wiley-Liss Inc. 2003): 1081–1101.

30. C. H. Turner, M. R. Forwood, J. Y. Rho, and T. Yoshikawa, "Mechanical Loading Thresholds for Lamellar and Woven Bone Formation," *Journal of Bone and Mineral Research* 9, no. 1 (1994): 87–97.

31. E. F. Morgan and T. M. Keaveny, "Dependence of Yield Strain of human Trabecular Bone on Anatomic Site," *Journal of Biomechanics* 34, no. 5 (2001): 569–577.

32. N. Kohli, J. C. Stoddart, and R. J. van Arkel, "The Limit of Tolerable Micromotion for Implant Osseointegration: A Systematic Review," *Scientific Reports* 11, no. 1 (2021): 1–11.

33. U. Simon, P. Augat, A. Ignatius, and L. Claes, "Influence of the Stiffness of Bone Defect Implants on the Mechanical Conditions at the Interface—A Finite Element Analysis with Contact," *Journal of Biomechanics* 36, no. 8 (2003): 1079–1086.

34. J. Henkel, M. A. Woodruff, D. R. Epari, et al., "Bone Regeneration Based on Tissue Engineering Conceptions — A 21st Century Perspective," *Bone Research* 1 (2013): 216–248.

35. J. Y. Rho, L. Kuhn-Spearing, and P. Zioupos, "Mechanical Properties and the Hierarchical Structure of Bone," *Medical Engineering & Physics* 20, no. 2 (1998): 92–102.

36. F. W. Wehrli, "Structural and Functional Assessment of Trabecular and Cortical Bone by Micro Magnetic Resonance Imaging," *Journal of Magnetic Resonance Imaging* 25 (2007): 390–409.

37. M. Sakai, H. Mutsuzaki, Y. Shimizu, Y. Okamoto, and T. Nakajima, "Two Case Reports Showing a Rather Striking Abnormal Finding of Unknown Origin Localized to the Cortex of an Amputated Femur," *Radiology Case Reports* 17, no. 12 (2022): 4874–4878.

38. R. Oftadeh, M. Perez-Viloria, J. C. Villa-Camacho, A. Vaziri, and A. Nazarian, "Biomechanics and Mechanobiology of Trabecular Bone: A Review," *Journal of Biomechanical Engineering* 137 (2015): 0108021–01080215.

39. M. Kothari, T. M. Keaveny, J. C. Lin, D. C. Newitt, H. K. Genant, and S. Majumdar, "Impact of Spatial Resolution on the Prediction of Trabecular Architecture Parameters," *Bone* 22, no. 5 (1998): 437–443.

40. N. L. Fazzalari and I. H. Parkinson, "Fractal Dimension and Architecture of Trabecular Bone," *The Journal of Pathology* 178, no. 1 (1996): 100–105.

41. S. J. Morrison and D. T. Scadden, "The Bone Marrow Niche for Haematopoietic Stem Cells," *Nature* 505 (2014): 327–334.

42. E. F. Morgan, H. H. Bayraktar, and T. M. Keaveny, "Trabecular bone modulus–density relationships depend on anatomic site," *Journal of Biomechanics* 36, no. 7 (2003): 897–904.

43. A. Garg and P. S. Walker, "The Effect of the Interface on the Bone Stresses beneath Tibial Components," *Journal of Biomechanics* 19, no. 12 (1986): 957–967.

44. S. A. Goldstein, D. L. Wilson, D. A. Sonstegard, and L. S. Matthews, "The Mechanical Properties of human Tibial Trabecular Bone as a Function of Metaphyseal Location," *Journal of Biomechanics* 16, no. 12 (1983): 965–969.

45. I. Hvid and S. L. Hansen, "Trabecular Bone Strength Patterns at the Proximal Tibial Epiphysis," *Journal of Orthopaedic Research* 3, no. 4 (1985): 464–472.

46. O. Lindahl, "Mechanical Properties of Dried Defatted Spongy Bone," *Acta Orthopaedica Scandinavica* 47, no. 1 (1976): 11–19.

47. A. Odgaard and F. Linde, "The underestimation of Young's modulus in compressive testing of cancellous bone specimens," *Journal of Biomechanics* 24, no. 8 (1991): 691–698.

48. T. M. Keaveny, R. E. Borchers, L. J. Gibson, and W. C. Hayes, "Trabecular Bone Modulus and Strength Can Depend on Specimen Geometry," *Journal of Biomechanics* 26, no. 8 (1993): 991–1000.

49. R. B. Ashman, J. Y. Rho, and C. H. Turner, "Anatomical Variation of Orthotropic Elastic Moduli of the Proximal human Tibia," *Journal of Biomechanics* 22, no. 8-9 (1989): 895–900.

50. S. M. Bentzen, I. Hvid, and J. Jorgensen, "Mechanical Strength of Tibial Trabecular Bone Evaluated by X-ray Computed Tomography," *Journal of Biomechanics* 20, no. 8 (1987): 743–752.

51. F. J. Klever, R. Klumpert, J. Horenberg, H. J. Grootenboer, D. H. Van Campen, and T. Pauly, "Global Mechanical Properties of Trabecular Bone: Experimental Determination and Prediction from a Structural Model," *Biomechanics: Current Interdisciplinary Research* (1985): 167–172.

52. A. Odgaard, I. Hvid, and F. Linde, "Compressive Axial Strain Distributions in Cancellous Bone Specimens," *Journal of Biomechanics* 22, no. 8-9 (1989): 829–835.

53. M. J. Munford, K. C. G. Ng, and J. R. T. Jeffers, "Mapping the Multi-Directional Mechanical Properties of Bone in the Proximal Tibia," *Advanced Functional Materials* 30, no. 46 (2020).

54. V. L. Giddings, G. S. Beaupré, R. T. Whalen, and D. R. Carter, "Calcaneal Loading during Walking and Running," *Medicine & Science in Sports & Exercise* 32, no. 3 (2000): 627–634.

55. K. E. S. Poole, L. Skingle, A. H. Gee, et al., "Focal Osteoporosis Defects Play a Key Role in Hip Fracture," *Bone* 94 (2017): 124–134.

56. D. R. Carter and W. C. Hayes, "The Compressive Behavior of Bone as a Two-phase Porous Structure," *Bone Jt Res Am* 59, no. 7 (1977): 954–962.

57. S. M. Nazemi, M. Amini, S. A. Kontulainen, et al., "Optimizing Finite Element Predictions of Local Subchondral Bone Structural Stiffness Using Neural Network-derived Density-modulus Relationships for Proximal Tibial Subchondral Cortical and Trabecular Bone," *Clinical Biomechanics* 41 (2017): 1–8.

58. J. D. Johnston, S. A. Kontulainen, B. A. Masri, and D. R. Wilson, "Predicting Subchondral Bone Stiffness Using a Depth-Specific CT Topographic Mapping Technique in Normal and Osteoarthritic Proximal Tibiae," *Clinical Biomechanics* 26, no. 10 (2011): 1012–1018.

59. V. D. Sherk and C. J. Rosen, "Senescent and Apoptotic Osteocytes and Aging: Exercise to the Rescue?," *Bone* 121 (2019): 255–258.

60. S. Ma, E. N. L. Goh, A. Jin, et al., "Long-term Effects of Bisphosphonate Therapy: Perforations, Microcracks and Mechanical Properties," *Scientific Reports* 7, no. 1 (2017): 43399.

61. T. P. Harrigan and R. W. Mann, "Characterization of Microstructural Anisotropy in Orthotropic Materials Using a Second Rank Tensor," *Journal of Materials Science* 19, no. 3 (1984): 761–767.

62. J. L. Williams and J. L. Lewis, "Properties and an Anisotropic Model of Cancellous Bone from the Proximal Tibial Epiphysis," *Journal of Biomechanical Engineering* 104, no. 1 (1982): 50–56.

63. F. Linde, B. Pongsoipetch, L. H. Frich, and I. Hvid, "Three-axial Strain Controlled Testing Applied to Bone Specimens from the Proximal Tibial Epiphysis," *Journal of Biomechanics* 23, no. 11 (1990): 1167–1172.

64. M. J. Ciarelli, S. A. Goldstein, J. L. Kuhn, D. D. Cody, and M. B. Brown, "Evaluation of Orthogonal Mechanical Properties and Density of human Trabecular Bone from the Major Metaphyseal Regions with Materials Testing and Computed Tomography," *Journal of Orthopaedic Research* 9, no. 5 (1991): 674–682.

65. P. K. Zysset, "A review of morphology–elasticity relationships in human trabecular bone: Theories and experiments," *Journal of Biomechanics* 36 (2003): 1469–1485.

66. S. M. Nazemi, D. M. L. Cooper, and J. D. Johnston, "Quantifying Trabecular Bone Material Anisotropy and Orientation Using Low Resolution Clinical CT Images: A Feasibility Study," *Medical Engineering & Physics* 38, no. 9 (2016): 978–987.

67. M. E. Kersh, P. K. Zysset, D. H. Pahr, U. Wolfram, D. Larsson, and M. G. Pandy, "Measurement of Structural Anisotropy in Femoral Trabecular Bone Using Clinical-resolution CT Images," *Journal of Biomechanics* 46, no. 15 (2013): 2659–2666.

68. H. A. Gray, F. Taddei, A. B. Zavatsky, L. Cristofolini, and H. S. Gill, "Experimental Validation of a Finite Element Model of a Human Cadaveric Tibia," 130 (2008): 031016.

69. A. Odgaard, J. Kabel, B. van Rietbergen, M. Dalstra, and R. Huiskes, "Fabric and Elastic Principal Directions of Cancellous Bone are Closely Related," *Journal of Biomechanics* 30 (1997): 487–495.

70. W. J. Whitehouse, "The Quantitative Morphology of Anisotropic Trabecular Bone," *Journal of Microscopy* 101, no. 2 (1974): 153–168.

71. T. P. Harrigan, M. Jasty, R. W. Mann, and W. H. Harris, "Limitations of the Continuum Assumption in Cancellous Bone," *Journal of Biomechanics* 21, no. 4 (1988): 269–275.

72. G. Maquer, S. N. Musy, J. Wandel, and T. Gross, "Bone Volume Fraction and Fabric Anisotropy Are Better Determinants of Trabecular Bone Stiffness Than Other Morphological Variables," *Journal of Bone and Mineral Research* 30, no. 6 (2015): 1000–1008.

73. P. Pivonka, A. Park, and M. R. Forwood, "Functional Adaptation of Bone: The Mechanostat and Beyond," *Multiscale Mechanobiology of Bone Remodeling and Adaptation*, ed. P. Pivonka, (CISM International Centre for Mechanical Sciences: Springer, 2018): 1–60, https://doi.org/10.1007/978-3-319-58845-2_1.

74. B. Subia, J. Kundu, and S. C, "Biomaterial Scaffold Fabrication Techniques for Potential Tissue Engineering Applications," *Tissue Engineering* 2010, 536.

75. M. F. Ashby, A. G. Evans, N. A. Fleck, L. J. Gibson, and J. W. Hutchinson, "Wadley HNG. Metal Foams: A Design Guide. Applied Mechanics Reviews," *Butterworth-Heinemann* (2001).

76. W. Huang, X. Li, X. Shi, and C. Lai, "Microsphere Based Scaffolds for Bone Regenerative Applications," *Biomaterials Science* 2, no. 9 (2014): 1145–1153.

77. T. Maconachie, M. Leary, B. Lozanovski, et al., "SLM Lattice Structures: Properties, Performance, Applications and Challenges," *Materials & Design* 183 (2019): 108137.

78. A. A. Zadpoor, "Additively Manufactured Porous Metallic Biomaterials," *Journal of Materials Chemistry B* 7, no. 26 (2019): 4088–4117.

79. C. Yan, L. Hao, A. Hussein, and P. Young, "Ti–6Al–4V triply periodic minimal surface structures for bone implants fabricated via selective laser melting," *Journal of the Mechanical Behavior of Biomedical Materials* 51 (2015): 61–73.

80. S. Ghouse, S. Babu, R. J. Van Arkel, K. Nai, P. A. Hooper, and J. R. T. Jeffers, "The Influence of Laser Parameters and Scanning Strategies on the Mechanical Properties of a Stochastic Porous Material," *Materials & Design* 131 (2017): 498–508.

81. H. Liang, L. Chao, D. Xie, et al., "Trabecular-like Ti–6Al–4V scaffold for bone repair: A diversified mechanical stimulation environment for bone regeneration," *Composites Part B: Engineering* 241 (2022): 110057.

82. J. Mueller, K. H. Matlack, K. Shea, and C. Daraio, "Energy Absorption Properties of Periodic and Stochastic 3D Lattice Materials," *Advanced Theory and Simulations* 2, no. 10 (2019): 1–11.

83. O. Al-Ketan and D. W. Lee, "Abu Al-Rub RK. Mechanical Properties of Additively-manufactured Sheet-based Gyroidal Stochastic Cellular Materials," *Additive Manufacturing* 48 (2021): 102418.

84. M. T. Hsieh, B. Endo, Y. Zhang, J. Bauer, and L. Valdevit, "The Mechanical Response of Cellular Materials with Spinodal Topologies," *Journal of the Mechanics and Physics of Solids* 125 (2019): 401–419.

85. S. Kumar, S. Tan, L. Zheng, and D. M. Kochmann, "Inverse-designed Spinodoid Metamaterials," *npj Computational Materials* 6, no. 1 (2020): 73.

86. H. Wang, Y. Lyu, J. Jiang, and H. Zhu, "Data-driven Inverse Design of Novel Spinodoid Bone Scaffolds with Highly Matched Mechanical Properties in Three Orthogonal Directions," *Materials & Design* 251 (2025): 113697.

87. S. Raghavendra, A. Molinari, A. Cao, et al., "Quasi-Static Compression and Compression–Compression Fatigue Behavior of Regular and Irregular Cellular Biomaterials," *Fatigue & Fracture of Engineering Materials & Structures* 44, no. 5 (2021): 1178–1194.

88. M. F. Ashby, "The Properties of Foams and Lattices," *Philosophical Transactions of the Royal Society A: Mathematical, Physical and Engineering Sciences* 364 (1838): 15–30.

89. C. Emmelmann, P. Scheinemann, M. Munsch, and V. Seyda, "Laser Additive Manufacturing of Modified Implant Surfaces with Osseointegrative Characteristics," *Physics Procedia* 12 (2011): 375–384.

90. J. Wu, W. Wang, and X. Gao, "Design and Optimization of Conforming Lattice Structures," *IEEE Transactions on Visualization and Computer Graphics* 27, no. 1 (2021): 43–56.

91. D. Li, W. Liao, N. Dai, and Y. M. Xie, "Comparison of Mechanical Properties and Energy Absorption of Sheet-based and Strut-based Gyroid Cellular Structures with Graded Densities," *Materials* 12, no. 13 (2019): 2183.

92. B. Sokollu, O. Gulcan, and E. I. Konukseven, "Mechanical Properties Comparison of Strut-based and Triply Periodic Minimal Surface Lattice Structures Produced by Electron Beam Melting," *Additive Manufacturing* 60 2022: 103199.

93. H. Barber, C. N. Kelly, K. Nelson, and K. Gall, "Compressive anisotropy of sheet and strut based porous Ti–6Al–4V scaffolds," *Journal of the Mechanical Behavior of Biomedical Materials* 115 (2021): 104243.

94. M. Araya, M. Jaskari, T. Rautio, T. Guillén, and A. Järvenpää, "Assessing the Compressive and Tensile Properties of TPMS-Gyroid and Stochastic Ti64 Lattice Structures: A Study on Laser Powder Bed Fusion Manufacturing for Biomedical Implants," *Journal of Science: Advanced Materials and Devices* 9, no. 1 (2024): 100663.

95. R. Wauthle, S. M. Ahmadi, S. Amin Yavari, et al., "Revival of Pure Titanium for Dynamically Loaded Porous Implants Using Additive Manufacturing," *Materials Science and Engineering: C* 54 (2015): 94–100.

96. L. J. Gibson and M. F. Ashby, "The Mechanics of Three-Dimensional Cellular Materials," *Proc R Soc Lond Ser Math Phys Sci* 382 (1982): 43–59, https://doi.org/10.1098/rspa.1982.0088.

97. L. J. Gibson and M. F. Ashby, Cellular Solids [Internet] (Cambridge University Press, 1997), https://www.cambridge.org/core/product/identifier/9781139878326/type/book.

98. O. Al-Ketan, R. Rowshan, and R. K. Abu Al-Rub, "Topology-mechanical Property Relationship of 3D Printed Strut, Skeletal, and Sheet Based Periodic Metallic Cellular Materials," *Additive Manufacturing* 19 (2018): 167–183.

99. S. Ahmadi, S. Yavari, R. Wauthle, et al., "Additively Manufactured Open-cell Porous Biomaterials Made from Six Different Space-filling Unit Cells: The Mechanical and Morphological Properties," *Materials* 8, no. 4 (2015): 1871–1896.

100. V. S. Deshpande, M. F. Ashby, and N. A. Fleck, "Foam Topology: Bending versus Stretching Dominated Architectures," *Acta Materialia* 49, no. 6 (2001): 1035–1040.

101. S. Kechagias, R. N. Oosterbeek, M. J. Munford, S. Ghouse, and J. R. T. Jeffers, "Controlling the Mechanical Behaviour of Stochastic Lattice Structures: The Key Role of Nodal Connectivity," *Additive Manufacturing* 54 (2022): 102730.

102. Y. Yamada, K. Shimojima, H. Hosokawa, Y. Chino, and M. Mabuchi, "Compressive Deformation Characteristics of Open-Cell Mg Alloys with Controlled Cell Structure," 43 (2002): 1298–1305.

103. S. J. Li, Q. S. Xu, Z. Wang, et al., "Influence of cell shape on mechanical properties of Ti–6Al–4V meshes fabricated by electron beam melting method," *Acta Biomaterialia* 10, no. 10 (2014): 4537–4547.

104. M. Leary, M. Mazur, H. Williams, et al., "Inconel 625 Lattice Structures Manufactured by Selective Laser Melting (SLM): Mechanical Properties, Deformation and Failure Modes," *Materials & Design* 157 (2018): 179–199.

105. S. Ghouse, S. Babu, K. Nai, P. A. Hooper, and J. R. T. Jeffers, "The Influence of Laser Parameters, Scanning Strategies and Material on the Fatigue Strength of a Stochastic Porous Structure," *Additive Manufacturing* 22 (2018): 290–301.

106. S. Ghouse, R. N. Oosterbeek, A. T. Mehmood, F. Vecchiato, D. Dye, and J. R. T. Jeffers, "Vacuum Heat Treatments of Titanium Porous Structures," *Additive Manufacturing* 47, no. April (2021): 102262.

107. S. M. Ahmadi, R. Kumar, E. V. Borisov, et al., "From Microstructural Design to Surface Engineering: A Tailored Approach for Improving Fatigue Life of Additively Manufactured Meta-biomaterials," *Acta Biomaterialia* 83 (2019): 153–166.

108. S. M. Ahmadi, G. Campoli, S. Amin Yavari, et al., "Mechanical Behavior of Regular Open-cell Porous Biomaterials Made of Diamond Lattice Unit Cells," *Journal of the Mechanical Behavior of Biomedical Materials* 34 (2014): 106–115.

109. D. Zhao, Y. Huang, Y. Ao, et al., "Effect of Pore Geometry on the Fatigue Properties and Cell Affinity of Porous Titanium Scaffolds Fabricated by Selective Laser Melting," *Journal of the Mechanical Behavior of Biomedical Materials* 88, no. August (2018): 478–487.

110. R. Brezny and D. J. Green, "Characterization of Edge Effects in Cellular Materials," *Journal of Materials Science* 25, no. 11 (1990): 4571–4578.

111. W. B. Anderson and R. S. Lakes, "Size Effects due to Cosserat Elasticity and Surface Damage in Closed-cell Polymethacrylimide Foam," *Journal of Materials Science* 29 (1994): 6413–6419.

112. C. Tekoğlu, L. J. Gibson, T. Pardoen, and P. R. Onck, "Size Effects in Foams: Experiments and Modeling," *Progress in Materials Science* 56, no. 2 (2011): 109–138.

113. P. R. Onck, E. W. Andrews, and L. J. Gibson, "Size Effects in Ductile Cellular Solids. Part I: Modeling," *International Journal of Mechanical Sciences* 43, no. 3 (2001): 681–699.

114. E. W. Andrews, G. Gioux, P. Onck, and L. J. Gibson, "Size Effects in Ductile Cellular Solids. Part II: Experimental Results," *International Journal of Mechanical Sciences* 43, no. 3 (2001): 701–713.

115. International Organization for Standardization. *ISO 13314:2011 Mechanical Testing of Metals – Ductility testing – Compression test for porous and cellular metals* (International Standard, 2011).

116. ASTM International, *ASTM D1621 – Standard Test Method for Compressive Properties Of Rigid Cellular Plastics* (2000).

117. S. Kechagias, K. J. Karunaseelan, R. N. Oosterbeek, and J. R. T. Jeffers, "The Coupled Effect of Aspect Ratio and Strut Micro-deformation Mode on the Mechanical Properties of Lattice Structures," *Mechanics of Materials* 191 (2024): 104944.

118. J. Bühring, J. Soika, M. Schirp-Schoenen, and K. U. Schröder, "Elastic Axial Stiffness Properties of Lattice Structures: Analytical Approach and Experimental Validation for Bcc and f2cc,Z Unit Cells," *Mechanics of Advanced Materials and Structures* 31 (2022): 1517–1533.

119. Y. Yang, M. Shan, L. Zhao, D. Qi, and J. Zhang, "Multiple Strut-deformation Patterns Based Analytical Elastic Modulus of Sandwich BCC Lattices," *Materials & Design* 181 (2019): 107916.

120. U. Hossain, S. Ghouse, K. Nai, and J. R. Jeffers, "Controlling and Testing Anisotropy in Additively Manufactured Stochastic Structures," *Additive Manufacturing* (2021): 39.

121. M. Munford, U. Hossain, S. Ghouse, and J. R. T. Jeffers, "Prediction of Anisotropic Mechanical Properties for Lattice Structures," *Additive Manufacturing* 32 (2020): 101041.

122. T. Tancogne-Dejean and D. Mohr, "Elastically-isotropic Truss Lattice Materials of Reduced Plastic Anisotropy," *International Journal of Solids and Structures* 138 (2018): 24–39.

123. V. Weißmann, R. Bader, H. Hansmann, and N. Laufer, "Influence of the Structural Orientation on the Mechanical Properties of Selective Laser Melted Ti6Al4V Open-porous Scaffolds," *Materials and Design* 95 (2016): 188–197.

124. A. Cuadrado, A. Yánez, O. Martel, S. Deviaene, and D. Monopoli, "Influence of Load Orientation and of Types of Loads on the Mechanical Properties of Porous Ti6Al4V Biomaterials," *Materials & Design* 135 (2017): 309–318.

125. S. Amirkhani, R. Z. Bagheri, and A. Yazdi, "Manipulating Failure Mechanism of Rapid Prototyped Scaffolds by Changing Nodal Connectivity and Geometry of the Pores," *Journal of Biomechanics* 45, no. 16 (2012): 2866–2875.

126. M. Smith, Z. Guan, and W. J. Cantwell, "Finite Element Modelling of the Compressive Response of Lattice Structures Manufactured Using the Selective Laser Melting Technique," *International Journal of Mechanical Sciences* 67 (2013): 28–41.

127. P. Wang, Y. Bian, F. Yang, H. Fan, and B. Zheng, "Mechanical Properties and Energy Absorption of FCC Lattice Structures with Different Orientation Angles," *Acta Mechanica* 231, no. 8 (2020): 3129–3144.

128. J. C. Wallach and L. J. Gibson, "Mechanical Behavior of a Three-dimensional Truss Material," *International Journal of Solids and Structures* 38, no. 40-41 (2001): 7181–7196.

129. S. Kechagias, K. Theodoridis, J. Broomfield, et al., "The Effect of Nodal Connectivity and Strut Density within Stochastic Titanium Scaffolds on Osteogenesis," *Frontiers in Bioengineering and Biotechnology* 11 (2023).

130. N. E. Dowling, "Mechanical Behavior of Materials, Engineering Methods for Deformation, Fracture, and Fatigue. Fourth," *Pearson* (2012): 954.

131. S. S. Manson and M. H. Hirschberg, "The Role of Ductility, Tensile Strength and Fracture Toughness in Fatigue," *Journal of the Franklin Institute* 290, no. 6 (1970): 539–548.

132. A. Turnbull, L. De, and E. R. Rios, "The Effect of Grain Size on THE Fatigue of Commercially Pure Aluminium," *Fatigue & Fracture of Engineering Materials & Structures* 18, no. 12 (1995): 1455–1467.

133. Y. Q. Chen, S. P. Pan, M. Z. Zhou, D. Q. Yi, D. Z. Xu, and Y. F. Xu, "Effects of Inclusions, Grain Boundaries and Grain Orientations on the Fatigue Crack Initiation and Propagation Behavior of 2524-T3 Al Alloy," *Materials Science and Engineering: A* 580 (2013): 150–158.

134. I. Bantounas, D. Dye, and T. C. Lindley, "The Effect of Grain Orientation on Fracture Morphology During High-Cycle Fatigue of Ti–6Al–4V," *Acta Materialia* 57, no. 12 (2009): 3584–3595.

135. X. Pan, S. Xu, G. Qian, et al., "The Mechanism of Internal Fatigue-crack Initiation and Early Growth in a Titanium Alloy with Lamellar and Equiaxed Microstructure," *Materials Science and Engineering: A* 798 (2020): 140110.

136. L. Christoph and M. Peters, "Titanium and Titanium Alloys : Fundamentals and Applications," *Wiley* (2006): 535.

137. R. Gnanamoorthy, Y. Mutoh, and Y. Mizuhara, "Fatigue Crack Growth Behavior of Equiaxed, Duplex and Lamellar Microstructure γ-base Titanium Aluminides," *Intermetallics* 4, no. 7 (1996): 525–532.

138. Y. L. Zhou and M. Niinomi, "Microstructures and mechanical properties of Ti–50mass% Ta alloy for biomedical applications," *Journal of Alloys and Compounds* 466, no. 1–2 (2008): 535–542.

139. F. Li, J. Li, T. Huang, H. Kou, and L. Zhou, "Compression Fatigue Behavior and Failure Mechanism of Porous Titanium for Biomedical Applications," *Journal of the Mechanical Behavior of Biomedical Materials* 65 (2017): 814–823.

140. N. W. Hrabe, P. Heinl, B. Flinn, C. Körner, and R. K. Bordia, "Compression-compression fatigue of selective electron beam melted cellular titanium (Ti-6Al-4V)," *Journal of Biomedical Materials Research Part B: Applied Biomaterials* 99B, no. 2 (2011): 313–320.

141. S. Amin Yavari, R. Wauthle, J. van der Stok, et al., "Fatigue Behavior of Porous Biomaterials Manufactured Using Selective Laser Melting," *Materials Science and Engineering: C* 33, no. 8 (2013): 4849–4858.

142. S. Zhao, S. J. Li, W. T. Hou, Y. L. Hao, R. Yang, and R. D. K. Misra, "The Influence of Cell Morphology on the Compressive Fatigue Behavior of Ti-6Al-4V Meshes Fabricated by Electron Beam Melting," *Journal of the Mechanical Behavior of Biomedical Materials* 59 (2016): 251–264.

143. C. Peng, P. Tran, H. Nguyen-Xuan, and A. J. M. Ferreira, "Mechanical Performance and Fatigue Life Prediction of Lattice Structures: Parametric Computational Approach," *Composite Structures* 235 (2020): 111821.

144. S. M. Ahmadi, R. Hedayati, Y. Li, et al., "Fatigue Performance of Additively Manufactured Meta-biomaterials: The Effects of Topology and Material Type," *Acta Biomaterialia* 65 (2018): 292–304.

145. M. Speirs, B. Van Hooreweder, J. Van Humbeeck, and J. P. Kruth, "Fatigue Behaviour of NiTi Shape Memory Alloy Scaffolds Produced by SLM, a Unit Cell Design Comparison," *Journal of the Mechanical Behavior of Biomedical Materials* 70 (2017): 53–59.

146. M. Pelegatti, F. Scalzo, F. Sordetti, et al., "Low Cycle Fatigue Behaviour of Cellular Materials: Experimental Comparative Study of Strut-based and Gyroid Structures Made of Additively Manufactured 316L Steel," *International Journal of Fatigue* 178 (2024): 108024.

147. Y. Zeng and W. Feng, "Metal Allergy in Patients with Total Hip Replacement: A Review," *Journal of International Medical Research* 41, no. 2 (2013): 247–252.

148. K. T. Kim, M. Y. Eo, T. T. H. Nguyen, and S. M. Kim, "General Review of Titanium Toxicity," *International Journal of Implant Dentistry* 5, no. 1 (2019).

149. M. Gasik, A. Braem, A. Chaudhari, J. Duyck, and J. Vleugels, "Titanium Implants with Modified Surfaces: Meta-analysis of in Vivo Osteointegration," *Materials Science and Engineering: C* 49 (2015): 152–158.

150. C. Kuphasuk, Y. Oshida, C. J. Andres, S. T. Hovijitra, M. T. Barco, and D. T. Brown, "Electrochemical Corrosion of Titanium and Titanium-based Alloys," *The Journal of Prosthetic Dentistry* 85, no. 2 (2001): 195–202.

151. G. Dong, J. Marleau-Finley, and Y. F. Zhao, "Investigation of Electrochemical Post-processing Procedure for Ti-6Al-4V Lattice Structure Manufactured by Direct Metal Laser Sintering (DMLS)," *The International Journal of Advanced Manufacturing Technology* 104, no. 9–12 (2019): 3401–3417.

152. F. A. Shah, M. Trobos, P. Thomsen, and A. Palmquist, "Commercially pure titanium (cp-Ti) versus titanium alloy (Ti6Al4V) materials as bone anchored implants — Is one truly better than the other?," *Materials Science and Engineering: C* 62 (2016): 960–966.

153. C. Y. Hu and T. R. Yoon, "Recent Updates for Biomaterials Used in Total Hip Arthroplasty," *Biomaterials Research BioMed Central Ltd* 22 (2018): 33.

154. B. R. Levine, S. Sporer, R. A. Poggie, C. J. Della Valle, and J. J. Jacobs, "Experimental and Clinical Performance of Porous Tantalum in Orthopedic Surgery," *Biomaterials* 27, no. 27 (2006): 4671–4681.

155. Y. Lu, T. Zhang, K. Chen, et al., "Application of Biodegradable Implants in Pediatric Orthopedics: Shifting from Absorbable Polymers to Biodegradable Metals," *Bioactive Materials* 50 (2025): 189–214.

156. Y. Yang, Y. Cheng, S. Peng, et al., "Microstructure Evolution and Texture Tailoring of Reduced Graphene Oxide Reinforced Zn Scaffold," *Bioactive Materials* 6, no. 5 (2021): 1230–1241.

157. R. Bonithon, C. Lupton, M. Roldo, et al., "Open-porous Magnesium-based Scaffolds Withstand in Vitro Corrosion under Cyclic Loading: A Mechanistic Study," *Bioactive Materials* 19 (2023): 406–417.

158. R. Dhandapani, P. D. Krishnan, A. Zennifer, et al., "Additive Manufacturing of Biodegradable Porous Orthopaedic Screw," *Bioactive Materials* 5, no. 3 (2020): 458–467.

159. J. Liu, B. Liu, S. Min, et al., "Biodegradable Magnesium Alloy WE43 Porous Scaffolds Fabricated by Laser Powder Bed Fusion for Orthopedic Applications: Process Optimization, in Vitro and in Vivo Investigation," *Bioactive Materials* 16 (2022): 301–319.

160. T. Rae, "The toxicity of metals used in orthopaedic prostheses. An experimental study using cultured human synovial fibroblasts," *The Journal of Bone and Joint Surgery British volume* 63-B, no. 3 (1981): 435–440.

161. V. Sansone, D. Pagani, and M. Melato, "The Effects on Bone Cells of Metal Ions Released from Orthopaedic Implants. A Review," *Clin Cases Miner Bone Metab* 10, no. 1 (2013): 34–40.

162. Å. S. Carlsson, B. Magnusson, and H. Möller, "Metal Sensitivity in Patients with Metal-To-Plastic Total Hip Arthroplasties," *Acta Orthopaedica Scandinavica* 51, no. 1–6 (1980): 57–62.

163. M. S. Caicedo, E. Solver, L. Coleman, J. J. Jacobs, and N. J. Hallab, "Females with Unexplained Joint Pain Following Total Joint Arthroplasty Exhibit a Higher Rate and Severity of Hypersensitivity to Implant Metals Compared with Males," *Journal of Bone and Joint Surgery* 99, no. 8 (2017): 621–628.

164. P. Thomas and S. Stea, *Metal Implant Allergy and Immuno-Allergological Compatibility Aspects of Ceramic Materials* (Springer, 2015).

165. A. Razak, A. D. Ebinesan, and C. P. Charalambous, "Metal Hypersensitivity in Patients with Conventional Orthopaedic Implants," *JBJS Reviews* 2, no. 2 (2014).

166. S. Van Bael, Y. C. Chai, S. Truscello, et al., "The Effect of Pore Geometry on the in Vitro Biological Behavior of human Periosteum-derived Cells Seeded on Selective Laser-melted Ti6Al4V Bone Scaffolds," *Acta Biomaterialia* 8, no. 7 (2012): 2824–2834.

167. C. Torres-Sanchez, J. M. Borgman, B. Sargeant, et al., "Comparison of Selective Laser Melted Commercially Pure Titanium Sheet-Based Triply Periodic Minimal Surfaces and Trabecular-Like Strut-Based Scaffolds for Tissue Engineering," *Advanced Engineering Materials* 24, no. 1 (2022): 2270002.

168. F. A. Shah, P. Thomsen, and A. Palmquist, "Osseointegration and Current Interpretations of the Bone-implant Interface," *Acta Biomaterialia* 84 (2019): 1–15.

169. N. Taniguchi, S. Fujibayashi, M. Takemoto, et al., "Effect of Pore Size on Bone Ingrowth into Porous Titanium Implants Fabricated by Additive Manufacturing: An in Vivo Experiment," *Materials Science and Engineering: C* 59 (2016): 690–701.

170. K.-H. Frosch, F. Barvencik, V. Viereck, et al., "Growth Behavior, Matrix Production, and Gene Expression of human Osteoblasts in Defined Cylindrical Titanium Channels," *Journal of Biomedical Materials Research Part A* 68A, no. 2 (2004): 325–334.

171. V. Karageorgiou and D. Kaplan, "Porosity of 3D Biomaterial Scaffolds and Osteogenesis," *Biomaterials* 26, no. 27 (2005): 5474–5491.

172. J. Markhoff, J. Wieding, V. Weissmann, J. Pasold, A. Jonitz-Heincke, and R. Bader, "Influence of Different Three-dimensional Open Porous Titanium Scaffold Designs on human Osteoblasts Behavior in Static and Dynamic Cell Investigations," *Materials* 8, no. 8 (2015): 5490–5507.

173. K. Man, M. Y. Brunet, S. Louth, et al., "Development of a Bone-Mimetic 3D Printed Ti6Al4V Scaffold to Enhance Osteoblast-Derived Extracellular Vesicles' Therapeutic Efficacy for Bone Regeneration," *Frontiers in Bioengineering and Biotechnology* 9 (2021): 757220.

174. M. Rumpler, A. Woesz, J. W. C. Dunlop, J. T. Van Dongen, and P. Fratzl, "The Effect of Geometry on Three-dimensional Tissue Growth," *Journal of The Royal Society Interface* 5, no. 27 (2008): 1173–1180.

175. C. M. Bidan, K. P. Kommareddy, M. Rumpler, P. Kollmannsberger, P. Fratzl, and J. W. C. Dunlop, "Geometry as a Factor for Tissue Growth: Towards Shape Optimization of Tissue Engineering Scaffolds," *Advanced Healthcare Materials* 2, no. 1 (2013): 186–194.

176. C. M. Nelson, R. P. Jean, J. L. Tan, et al., "Emergent Patterns of Growth Controlled by Multicellular Form and Mechanics," *Proceedings of the National Academy of Sciences* 102, no. 33 (2005): 11594–11599.

177. S. J. P. Callens, R. J. C. Uyttendaele, L. E. Fratila-Apachitei, and A. A. Zadpoor, "Substrate Curvature as a Cue to Guide Spatiotemporal Cell and Tissue Organization," *Biomaterials* 232 (2020): 119739.

178. J. Knychala, N. Bouropoulos, C. J. Catt, O. L. Katsamenis, C. P. Please, and B. G. Sengers, "Pore Geometry Regulates Early Stage human Bone Marrow Cell Tissue Formation and Organisation," *Annals of Biomedical Engineering* 41, no. 5 (2013): 917–930.

179. P. R. Buenzli, M. Lanaro, C. S. Wong, et al., "Cell Proliferation and Migration Explain Pore Bridging Dynamics in 3D Printed Scaffolds of Different Pore Size," *Acta Biomaterialia* 114 (2020): 285–295.

180. K. C. Nune, R. D. K. Misra, S. J. Li, Y. L. Hao, and R. Yang, "C ellular response of osteoblasts to low modulus Ti-24Nb-4Zr-8Sn alloy mesh structure," *Journal of Biomedical Materials Research Part A* 105 (2016): 859–870.

181. V. Vogel and M. Sheetz, "Local Force and Geometry Sensing Regulate Cell Functions," *Nature Reviews Molecular Cell Biology* 7 (2006): 265–275.

182. C. Wang, D. Xu, L. Lin, et al., "Large-pore-size Ti6Al4V Scaffolds with Different Pore Structures for Vascularized Bone Regeneration," *Materials Science and Engineering: C* 131 (2021): 112499.

183. J. Jiao, Q. Hong, D. Zhang, et al., "Influence of Porosity on Osteogenesis, Bone Growth and Osteointegration in Trabecular Tantalum Scaffolds Fabricated by Additive Manufacturing," *Frontiers in Bioengineering and Biotechnology* 11 (2023).

184. N. Reznikov, H. Chase, Y. Ben Zvi, et al., "Inter-trabecular Angle: A Parameter of Trabecular Bone Architecture in the human Proximal Femur That Reveals Underlying Topological Motifs," *Acta Biomaterialia* 44 (2016): 65–72.

185. J. Van der Stok, O. P. Van der Jagt, S. Amin Yavari, et al., "Selective Laser Melting-Produced Porous Titanium Scaffolds Regenerate Bone in Critical Size Cortical Bone Defects," *Journal of Orthopaedic Research* 31, no. 5 (2013): 792–799.

186. A. Feldman, M. Assad, M. B. Davies, J. Mangwani, E. Alabort, and M. Tuncer, "Cortico-Cancellous Osseointegration into Additively Manufactured Titanium Implants Using a Load-bearing Femoral Ovine Model," *Frontiers in Bioengineering and Biotechnology* 12 (2024).

187. N. Reznikov, O. R. Boughton, S. Ghouse, et al., "Individual Response Variations in Scaffold-Guided Bone Regeneration Are Determined by Independent Strain- and Injury-Induced Mechanisms," *Biomaterials* 194 (2019): 183–194.

188. S. M. Van Gaalen, M. C. Kruyt, R. E. Geuze, J. D. De Bruijn, J. Alblas, and W. J. A. Dhert, "Use of Fluorochrome Labels in in Vivo Bone Tissue Engineering Research," *Tissue Engineering Part B: Reviews* 16, no. 2 (2010): 209–217.

189. P. Ouyang, H. Dong, X. He, et al., "Hydromechanical Mechanism behind the Effect of Pore Size of Porous Titanium Scaffolds on Osteoblast Response and Bone Ingrowth," *Materials & Design* 183 (2019): 108151.

190. Z. Chen, X. Yan, S. Yin, et al., "Influence of the Pore Size and Porosity of Selective Laser Melted Ti6Al4V ELI Porous Scaffold on Cell Proliferation, Osteogenesis and Bone Ingrowth," *Materials Science and Engineering: C* 106 (2020): 110289.

191. Y. Zhang, N. Sun, M. Zhu, et al., "The Contribution of Pore Size and Porosity of 3D Printed Porous Titanium Scaffolds to Osteogenesis," *Biomater Adv* (2022): 133.

192. X. Wang, D. Zhang, H. Peng, J. Yang, Y. Li, and J. Xu, "Optimize the Pore Size-Pore Distribution-Pore Geometry-Porosity of 3D-printed Porous Tantalum to Obtain Optimal Critical Bone Defect Repair Capability," *Biomaterials Advances* 154 (2023): 213638.

193. R. E. Laureijs, J. B. Roca, S. P. Narra, C. Montgomery, J. L. Beuth, and E. R. H. Fuchs, "Metal Additive Manufacturing: Cost Competitive beyond Low Volumes," *Journal of Manufacturing Science and Engineering* 139, no. 8 (2017): 1–9.

194. S. Singh and S. Ramakrishna, "Biomedical Applications of Additive Manufacturing: Present and Future," *Current Opinion in Biomedical Engineering* 2 (2017): 105–115.

195. E. Maleki, S. Bagherifard, M. Bandini, and M. Guagliano, "Surface Post-treatments for Metal Additive Manufacturing: Progress, Challenges, and Opportunities," *Additive Manufacturing* 37 (2021): 101619.

196. International Organization for Standardization, ASTM. ISO/ASTM 52900:2017 Additive manufacturing – General principles – Terminology 2017. 1–19.

197. International Organization for Standardization. ISO-17296-2-2015 2015.

198. I. Gibson, D. Rosen, B. Stucker, and M. Khorasani, *Additive Manufacturing Technologies. Additive Manufacturing Technologies* (Springer International Publishing, 2021).

199. A. Bournias-Varotsis, X. Han, R. A. Harris, and D. S. Engstrøm, "Ultrasonic Additive Manufacturing Using Feedstock with Build-in Circuitry for 3D Metal Embedded Electronics," *Additive Manufacturing* 29 (2019): 100799.

200. D. Chekkaramkodi, L. Jacob, C. MS, R. Umer, and H. Butt, "Review of Vat Photopolymerization 3D Printing of Photonic Devices," *Additive Manufacturing* 86 (2024): 104189.

201. S. M. Yusuf and N. Gao, "Influence of Energy Density on Metallurgy and Properties in Metal Additive manufacturing," *Materials Science and Technology* 33 (2017): 1269–1289.

202. I. Echeta, X. Feng, B. Dutton, R. Leach, and S. Piano, "Review of Defects in Lattice Structures Manufactured by Powder Bed Fusion," *The International Journal of Advanced Manufacturing Technology* 106, no. 5–6 (2020): 2649–2668.

203. J. Metelkova, L. Vanmunster, H. Haitjema, and B. Van Hooreweder, "Texture of Inclined Up-facing Surfaces in Laser Powder Bed Fusion of Metals," *Additive Manufacturing* 42 (2021): 101970.

204. P. Mercelis and J. P. Kruth, "Residual Stresses in Selective Laser Sintering and Selective Laser Melting," *Rapid Prototyping Journal* 12, no. 5 (2006): 254–265.

205. K. Carpenter and A. Tabei, "On Residual Stress Development, Prevention, and Compensation in Metal Additive Manufacturing," *Materials* 13, no. 2 (2020): 255.

206. L. Liu, P. Kamm, F. García-Moreno, J. Banhart, and D. Pasini, "Elastic and Failure Response of Imperfect Three-dimensional Metallic Lattices: The Role of Geometric Defects Induced by Selective Laser Melting," *Journal of the Mechanics and Physics of Solids* 107 (2017): 160–184.

207. Y. Lu, Z. Cui, L. Cheng, et al., "Quantifying the Discrepancies in the Geometric and Mechanical Properties of the Theoretically Designed and Additively Manufactured Scaffolds," *Journal of the Mechanical Behavior of Biomedical Materials* 112 (2020): 104080.

208. Y. Amani, S. Dancette, P. Delroisse, A. Simar, and E. Maire, "Compression Behavior of Lattice Structures Produced by Selective Laser Melting: X-ray Tomography Based Experimental and Finite Element Approaches," *Acta Materialia* 159 (2018): 395–407.

209. R. S. Thanumoorthy, J. K. Chaurasia, V. Anil Kumar, P. I. Pradeep, et al., "Effect of Build Orientation on Anisotropy in Tensile Behavior of Laser Powder Bed Fusion Fabricated SS316L," *Journal of Materials Engineering and Performance* 33 (2023): 7930–7943.

210. J. Yoshioka and M. Eshraghi, "Temporal Evolution of Temperature Gradient and Solidification Rate in Laser Powder Bed Fusion Additive Manufacturing," *Heat and Mass Transfer* 59, no. 7 (2023): 1155–1166.

211. T. DebRoy, H. L. Wei, J. S. Zuback, et al., "Additive manufacturing of metallic components – Process, structure and properties," *Progress in Materials Science* 92 (2018): 112–224.

212. Y. Kok, X. P. Tan, P. Wang, et al., "Anisotropy and Heterogeneity of Microstructure and Mechanical Properties in Metal Additive Manufacturing: A Critical Review," *Materials & Design* 139 (2018): 565–586.

213. E. Pehlivan, M. Roudnicka, J. Dzugan, et al., "Effects of Build Orientation and Sample Geometry on the Mechanical Response of Miniature CP-Ti Grade 2 Strut Samples Manufactured by Laser Powder Bed Fusion," *Additive Manufacturing* 35 (2020): 101403.

214. X. Cao, L. N. Carter, K. Man, V. M. Villapún, L. Giangiorgi, and S. C. Cox, "Improving predictability of additively manufactured Ti-6Al-4 V lattices for orthopaedic devices: A parametric and struts angle study," *Materials & Design* 243 (2024): 113043.

215. U. Hossain, S. Ghouse, K. Nai, and J. R. T. Jeffers, "Mechanical and Morphological Properties of Additively Manufactured SS316L and Ti6Al4V Micro-struts as a Function of Build Angle," *Additive Manufacturing* 46 (2021): 102050.

216. Z. Dong, Y. Liu, W. Li, and J. Liang, "Orientation Dependency for Microstructure, Geometric Accuracy and Mechanical Properties of Selective Laser Melting AlSi10Mg Lattices," *Journal of Alloys and Compounds* 791 (2019): 490–500.

217. M. Baier, M. Sinico, A. Witvrouw, W. Dewulf, and S. Carmignato, "A Novel Tomographic Characterisation Approach for Sag and Dross Defects in Metal Additively Manufactured Channels," *Additive Manufacturing* 39 (2021): 101892.

218. A. Charles, A. Elkaseer, U. Paggi, L. Thijs, V. Hagenmeyer, and S. Scholz, "Down-facing Surfaces in Laser Powder Bed Fusion of Ti6Al4V: Effect of Dross Formation on Dimensional Accuracy and Surface Texture," *Additive Manufacturing* 46 (2021): 102148.

219. L. Thijs, F. Verhaeghe, T. Craeghs, J. V. Humbeeck, and J. P. Kruth, "A Study of the Microstructural Evolution During Selective Laser Melting of Ti–6Al–4V," *Acta Materialia* 58, no. 9 (2010): 3303–3312.

220. S. Tsopanos, R. A. W. Mines, S. McKown, et al., "The Influence of Processing Parameters on the Mechanical Properties of Selectively Laser Melted Stainless Steel Microlattice Structures," *Journal of Manufacturing Science and Engineering* 132, no. 4 (2010): 0410111–04101112.

221. L. Cordova, M. Campos, and T. Tinga, "Revealing the Effects of Powder Reuse for Selective Laser Melting by Powder Characterization," *Jom Journal of the Minerals Metals and Materials Society* 71, no. 3 (2019): 1062–1072.

222. Y. Guo, C. Chen, Q. Wang, and M. Liu, "Effects of Reuse on the Properties of Tantalum Powders and Tantalum Parts Additively Manufactured by Electron Beam Powder Bed Fusion," *Mater Res Express* 8, no. 4 (2021).

223. A. C. Jones, J. R. T. Jeffers, and R. N. Oosterbeek, "Frequency Dependent Fatigue Behaviour of Additively Manufactured Titanium Lattices," *Engineering Failure Analysis* 152 (2023): 107475.

224. B. Wysocki, P. Maj, R. Sitek, J. Buhagiar, K. J. Kurzydłowski, and W. Świeszkowski, "Laser and Electron Beam Additive Manufacturing Methods of Fabricating Titanium Bone Implants," *Applied Sciences (Switzerland)* 7, no. 7 (2017).

225. A. Nicum, A. Di Laura, H. Hothi, J. Henckel, K. Schlueter-Brust, and A. Hart, "Surface adhered titanium particles on 3D printed off-the-shelf acetabular cups," *Journal of Orthopaedic Research* 42 (2024): 2817–2825.

226. P. K. Gokuldoss, S. Kolla, and J. Eckert, "Additive Manufacturing Processes: Selective Laser Melting, Electron Beam Melting and Binder Jetting—Selection Guidelines," *Materials* 10 (2017): 672.

227. H. K. Rafi, N. V. Karthik, H. Gong, T. L. Starr, and B. E. Stucker, "Microstructures and Mechanical Properties of Ti6Al4V Parts Fabricated by Selective Laser Melting and Electron Beam Melting," *Journal of Materials Engineering and Performance* 22, no. 12 (2013): 3872–3883.

228. Y. J. Liu, S. J. Li, H. L. Wang, et al., "Microstructure, Defects and Mechanical Behavior of Beta-type Titanium Porous Structures Manufactured by Electron Beam Melting and Selective Laser Melting," *Acta Materialia* 113 (2016): 56–67.

229. J. Metelkova, Y. Kinds, K. Kempen, C. de Formanoir, A. Witvrouw, and B. Van Hooreweder, "On the Influence of Laser Defocusing in Selective Laser Melting of 316L," *Additive Manufacturing* 23 (2018): 161–169.

230. I. Yadroitsev, L. Thivillon, P. Bertrand, and I. Smurov, "Strategy of Manufacturing Components with Designed Internal Structure by Selective Laser Melting of Metallic Powder," *Applied Surface Science* 254, no. 4 (2007): 980–983.

231. M. Tang, P. C. Pistorius, and J. L. Beuth, "Prediction of Lack-of-fusion Porosity for Powder Bed Fusion," *Additive Manufacturing* 14 (2017): 39–48.

232. M. Zhang, C.-N. Sun, X. Zhang, et al., "Fatigue and Fracture Behaviour of Laser Powder Bed Fusion Stainless Steel 316L: Influence of Processing Parameters," *Materials Science and Engineering: A* 703 (2017): 251–261.

233. S. Pereira, A. I. F. Vaz, and L. N. Vicente, "On the Optimal Object Orientation in Additive Manufacturing," *The International Journal of Advanced Manufacturing Technology* 98, no. 5–8 (2018): 1685–1694.

234. W. E. King, H. D. Barth, V. M. Castillo, et al., "Observation of Keyhole-mode Laser Melting in Laser Powder-bed Fusion Additive Manufacturing," *Journal of Materials Processing Technology* 214, no. 12 (2014): 2915–2925.

235. H. Gong, K. Rafi, H. Gu, T. Starr, and B. Stucker, "Analysis of Defect Generation in Ti–6Al–4V parts Made Using Powder Bed Fusion Additive Manufacturing Processes," *Additive Manufacturing* 1–4 (2014): 87–98.

236. C. Qiu, S. Yue, N. J. E. Adkins, et al., "Influence of Processing Conditions on Strut Structure and Compressive Properties of Cellular Lattice Structures Fabricated by Selective Laser Melting," *Materials Science and Engineering: A* 628 (2015): 188–197.

237. G. Yang, C. Li, C. Wang, et al., "Multi-scale Optimization of PBF-LB/M Mg-Zn-Gd Alloys: Synergistic Enhancement of Corrosion Resistance and Mechanical Properties for Bone Implants," *Journal of Alloys and Compounds* 1034 (2025): 181425.

238. F. Bartolomeu, O. Carvalho, M. Gasik, and F. S. Silva, "Multifunctional Ti6Al4V-CoCrMo implants fabricated by multi-material laser powder bed fusion technology: A disruptive material's design and manufacturing philosophy," *Journal of the Mechanical Behavior of Biomedical Materials* 138 (2023): 105583.

239. J. C. Griffis, K. Shahed, K. Meinert, B. Yilmaz, M. Lear, and G. Manogharan, "Multi-material Laser Powder Bed Fusion: Effects of Build Orientation on Defects, Material Structure and Mechanical Properties," *npj Advanced Manufacturing* 2, no. 1 (2025): 5.

240. L. Vanmunster, L. R. Goossens, L. Sergeant, B. Van Hooreweder, and B. Vrancken, "Adaptive Slicing for Increased Productivity of Metal Laser Powder Bed Fusion," *Additive Manufacturing* 112 (2025): 105000.

241. V. Holla, P. Kopp, J. Grünewald, K. Wudy, and S. Kollmannsberger, "Laser Beam Shape Optimization in Powder Bed Fusion of Metals," *Additive Manufacturing* 72 (2023): 103609.

242. Z. Li, Z. Zhang, S. Zhang, et al., "In-situ Monitoring in Laser Powder Bed Fusion Based on Acoustic Signal Time-frequency Synchrosqueezing Transform and Multi-scale Spatially Interactive Fusion Convolutional Neural Network," *Journal of Manufacturing Processes* 126 (2024): 471–486.

243. F. Nahr, T. Novotny, D. Kunz, et al., "Advanced Process Control in Laser-Based Powder Bed Fusion–Smart Fusion Feedback-Loop Control as a Path to Uniform Properties for Complex Structures?," *Journal of Materials Research and Technology* 34 (2025): 604–618.

244. V. Karkaria, A. Goeckner, R. Zha, et al., "Towards a Digital Twin Framework in Additive Manufacturing: Machine Learning and Bayesian Optimization for Time Series Process Optimization," *Journal of Manufacturing Systems* 75 (2024): 322–332.

245. M. Dallago, B. Winiarski, F. Zanini, S. Carmignato, and M. Benedetti, "On the Effect of Geometrical Imperfections and Defects on the Fatigue Strength of Cellular Lattice Structures Additively Manufactured via Selective Laser Melting," *International Journal of Fatigue* 124 (2019): 348–360.

246. A. Cutolo, B. Neirinck, K. Lietaert, C. de Formanoir, and B. Van Hooreweder, "Influence of Layer Thickness and Post-process Treatments on the Fatigue Properties of CoCr Scaffolds Produced by Laser Powder Bed Fusion," *Additive Manufacturing* 23, no. June (2018): 498–504.

247. G. Pyka, G. Kerckhofs, I. Papantoniou, M. Speirs, J. Schrooten, and M. Wevers, "Surface Roughness and Morphology Customization of Additive Manufactured Open Porous Ti6Al4V Structures," *Materials* 6, no. 10 (2013): 4737–4757.

248. C. O'Keeffe, M. Kotlarz, I. F. Gonçalves, C. Lally, and D. J. Kelly, "Chemical Etching of Ti-6Al-4V Biomaterials Fabricated by Selective Laser Melting Enhances Mesenchymal Stromal Cell Mineralization," *J Biomed Mater Res - Part A* 112, no. 9 (2024): 1548–1564.

249. B. Van Hooreweder, Y. Apers, K. Lietaert, and J. P. Kruth, "Improving the Fatigue Performance of Porous Metallic Biomaterials Produced by Selective Laser Melting," *Acta Biomaterialia* 47 (2017): 193–202.

250. B. Van Hooreweder, K. Lietaert, B. Neirinck, N. Lippiatt, and M. Wevers, "CoCr F75 Scaffolds Produced by Additive Manufacturing: Influence of Chemical Etching on Powder Removal and Mechanical Performance," *Journal of the Mechanical Behavior of Biomedical Materials* 68 (2017): 216–223.

251. C. O'Keeffe, D. Taylor, C. Lally, and D. J. Kelly, "Morphological Induced Improvements in the Bulk Mechanical Properties of Chemically Etched Additively Manufactured Ti-6Al-4V Micro-struts," *Additive Manufacturing* 75 (2023): 103748.

252. B. Wysocki, J. Idaszek, J. Buhagiar, et al., "The Influence of Chemical Polishing of Titanium Scaffolds on Their Mechanical Strength and In-Vitro Cell Response," *Materials Science and Engineering: C* 95 (2019): 428–439.

253. R. N. Oosterbeek, G. Sirbu, S. Hansal, K. Nai, and J. R. T. Jeffers, "Effect of chemical–electrochemical surface treatment on the roughness and fatigue performance of porous titanium lattice structures," *Additive Manufacturing* 78 (2023): 103896.

254. B. Van Hooreweder and J. P. Kruth, "Advanced Fatigue Analysis of Metal Lattice Structures Produced by Selective Laser Melting," *CIRP Annals* 66, no. 1 (2017): 221–224.

255. W. Yuan, W. Hou, S. Li, et al., "Heat Treatment Enhancing the Compressive Fatigue Properties of Open-cellular Ti-6Al-4V Alloy Prototypes Fabricated by Electron Beam Melting," *Journal of Materials Science & Technology* 34, no. 7 (2018): 1127–1131.

256. K. Karami, A. Blok, L. Weber, et al., "Continuous and Pulsed Selective Laser Melting of Ti6Al4V Lattice Structures: Effect of Post-processing on Microstructural Anisotropy and Fatigue Behaviour," *Additive Manufacturing* 36, no. June (2020): 101433.

257. A. M. C. Barradas, H. Yuan, C. A. van Blitterswijk, and P. Habibovic, "Osteoinductive Biomaterials: Current Knowledge of Properties, Experimental Models and Biological Mechanisms," *European Cells and Materials* 21 (2011): 407–429.

258. O. Andrukhov, R. Huber, B. Shi, et al., "Proliferation, Behavior, and Differentiation of Osteoblasts on Surfaces of Different Microroughness," *Dental Materials* 32, no. 11 (2016): 1374–1384.

259. D. D. Deligianni, N. Katsala, S. Ladas, D. Sotiropoulou, J. Amedee, and Y. F. Missirlis, "Effect of Surface Roughness of the Titanium alloy Ti–6Al–4V on Human Bone Marrow Cell Response and on Protein Adsorption," *Biomaterials* 22, no. 11 (2001): 1241–1251.

260. J. I. Rosales-Leal, M. A. Rodríguez-Valverde, G. Mazzaglia, et al., "Effect of Roughness, Wettability and Morphology of Engineered Titanium Surfaces on Osteoblast-like Cell Adhesion," *Colloids and Surfaces A: Physicochemical and Engineering Aspects* 365, no. 1–3 (2010): 222–229.

261. M. Bigerelle, K. Anselme, B. Noël, I. Ruderman, P. Hardouin, and A. Iost, "Improvement in the Morphology of Ti-based Surfaces: A New Process to Increase in Vitro human Osteoblast Response," *Biomaterials* 23, no. 7 (2002): 1563–1577.

262. L. Prodanov, J. te Riet, E. Lamers, et al., "The Interaction between Nanoscale Surface Features and Mechanical Loading and Its Effect on Osteoblast-like Cells Behavior," *Biomaterials* 31, no. 30 (2010): 7758–7765.

263. R. J. McMurray, N. Gadegaard, P. M. Tsimbouri, et al., "Nanoscale Surfaces for the Long-term Maintenance of Mesenchymal Stem Cell Phenotype and Multipotency," *Nature Materials* 10, no. 8 (2011): 637–644.

264. N. Cruz, M. I. Martins, J. D. Santos, J. G. Mur, and J. P. Tondela, "Surface Comparison of Three Different Commercial Custom-made Titanium Meshes Produced by SLM for Dental Applications," *Materials* 13, no. 9 (2020): 2177.

265. V. Máša, D. Horňák, and D. Petrilák, "Industrial Use of Dry Ice Blasting in Surface Cleaning," *Journal of Cleaner Production* 329 (2021): 129630.

266. D. Velten, V. Biehl, F. Aubertin, B. Valeske, W. Possart, and J. Breme, "Preparation of TiO_2 layers on cp-Ti and Ti_6Al_4V by thermal and anodic oxidation and by sol-gel coating techniques and their characterization," *Journal of Biomedical Materials Research* 59, no. 1 (2002): 18–28.

267. H. Tsujita, H. Nishizaki, A. Miyake, S. Takao, and S. Komasa, "Effect of Plasma Treatment on Titanium Surface on the Tissue Surrounding Implant Material," *International Journal of Molecular Sciences* 22, no. 13 (2021): 6931.

268. A. Toffoli, L. Parisi, M. G. Bianchi, S. Lumetti, O. Bussolati, and G. M. Macaluso, "Thermal Treatment to Increase Titanium Wettability Induces Selective Proteins Adsorption from Blood Serum Thus Affecting Osteoblasts Adhesion," *Materials Science and Engineering: C* 107 (2020): 110250.

269. H. Güleryüz and H. Çimenoğlu, "Effect of Thermal Oxidation on Corrosion and Corrosion–wear Behaviour of a Ti–6Al–4V Alloy," *Biomaterials* 25, no. 16 (2004): 3325–3333.

270. T. Kokubo, F. Miyaji, H. M. Kim, and T. Nakamura, "Spontaneous Formation of Bonelike Apatite Layer on Chemically Treated Titanium Metals," *Journal of the American Ceramic Society* 79, no. 4 (1996): 1127–1129.

271. J. Jakubowicz, G. Adamek, and L. Smardz, "Porous Surface State Analysis of Anodized Titanium for Biomedical Applications," *Metallurgical and Materials Transactions A* 53, no. 1 (2022): 86–94.

272. C. Kim, M. R. Kendall, M. A. Miller, et al., "Comparison of Titanium Soaked in 5 M NaOH or 5 M KOH Solutions," *Materials Science and Engineering: C* 33, no. 1 (2013): 327–339.

273. F. M. He, G. L. Yang, Y. N. Li, X. X. Wang, and S. F. Zhao, "Early Bone Response to Sandblasted, Dual Acid-etched and H2O2/HCl Treated Titanium Implants: An Experimental Study in the Rabbit," *International Journal of Oral and Maxillofacial Surgery* 38, no. 6 (2009): 677–681.

274. S. Nishiguchi, H. Kato, H. Fujita, et al., "Titanium Metals Form Direct Bonding to Bone after Alkali and Heat Treatments," *Biomaterials* 22, no. 18 (2001): 2525–2533.

275. M. Takemoto, S. Fujibayashi, M. Neo, et al., "Osteoinductive Porous Titanium Implants: Effect of Sodium Removal by Dilute HCl Treatment," *Biomaterials* 27, no. 13 (2006): 2682–2691.

276. R. Rovetta, P. Ginestra, R. M. Ferraro, K. Zohar-Hauber, S. Giliani, and E. Ceretti, "Building Orientation and Post Processing of Ti6Al4V

Produced by Laser Powder Bed Fusion Process," *J Manuf Mater Process* 7, no. 1 (2023).

277. H. Wang, Y. I. Wan, M. Yu, et al., "Complete Removal of Residual Particles and Realization of Mechanical Properties to Improve Osseointegration in Additively Manufactured Ti6Al4 V Scaffolds through Flowing Acid Etching," *ACS Biomaterials Science & Engineering* 10, no. 5 (2024): 3454–3469.

278. D. M. Vasconcelos, S. G. Santos, M. Lamghari, and M. A. Barbosa, "The Two Faces of Metal Ions: From Implants Rejection to Tissue Repair/Regeneration," *Biomaterials* 84 (2016): 262–275.

279. C. Schopper, D. Moser, W. Goriwoda, et al., "The effect of three different calcium phosphate implant coatings on bone deposition and coating resorption: A long-term histological study in sheep," *Clinical Oral Implants Research* 16, no. 3 (2005): 357–368.

280. T. Jinno, D. T. Davy, and V. M. Goldberg, "Comparison of Hydroxyapatite and Hydroxyapatite Tricalcium-phosphate Coatings," *The Journal of Arthroplasty* 17, no. 7 (2002): 902–909.

281. R. Drevet and H. Benhayoune, "Electrodeposition of Calcium Phosphate Coatings on Metallic Substrates for Bone Implant Applications: A Review," *Coatings* 12 (2022): 539.

282. T. M. Lee, B. C. Wang, Y. C. Yang, E. Chang, and C. Y. Yang, "Comparison of Plasma-sprayed Hydroxyapatite Coatings and Hydroxyapatite/Tricalcium Phosphate Composite Coatings: In Vivo Study," *Journal of Biomedical Materials Research* 55, no. 3 (2001): 360–367.

283. T. Goto, T. Kojima, T. Iijima, et al., "Resorption of Synthetic Porous Hydroxyapatite and Replacement by Newly Formed Bone," *Journal of Orthopaedic Science* 6 (2001): 444–447.

284. F. Schönweger, C. M. Sprecher, S. Milz, et al., "New Insights into Osteointegration and Delamination from a Multidisciplinary Investigation of a Failed Hydroxyapatite-coated Hip Joint Replacement," *Materials* 13, no. 21 (2020): 1–17.

285. H. Ao, Y. Xie, H. Tan, et al., "Improved hMSC Functions on Titanium Coatings by Type I Collagen Immobilization," *Journal of Biomedical Materials Research Part A* 102, no. 1 (2014): 204–214.

286. S. Rammelt, E. Schulze, R. Bernhardt, et al., "Coating of titanium implants with type-I collagen," *Journal of Orthopaedic Research* 22, no. 5 (2004): 1025–1034.

287. Y. Ku, C. P. Chung, and J. H. Jang, "The Effect of the Surface Modification of Titanium Using a Recombinant Fragment of Fibronectin and Vitronectin on Cell Behavior," *Biomaterials* 26, no. 25 (2005): 5153–5157.

288. B. Wildemann, F. Kandziora, G. Krummrey, et al., "Local and Controlled Release of Growth Factors (combination of IGF-I and TGF-beta I, and BMP-2 alone) from a Polylactide Coating of Titanium Implants Does Not Lead to Ectopic Bone Formation in Sheep Muscle," *Journal of Controlled Release* 95, no. 2 (2004): 249–256.

289. S. E. Kim, Y. P. Yun, J. Y. Lee, J. S. Shim, K. Park, and J. B. Huh, "Co-delivery of Platelet-derived Growth Factor (PDGF-BB) and Bone Morphogenic Protein (BMP-2) Coated onto Heparinized Titanium for Improving Osteoblast Function and Osteointegration," *Journal of Tissue Engineering and Regenerative Medicine* 9, no. 12 (2015): E219–E228.

290. Z. Shi, K. G. Neoh, E. T. Kang, C. Poh, and W. Wang, "Titanium with Surface-Grafted Dextran and Immobilized Bone Morphogenetic Protein-2 for Inhibition of Bacterial Adhesion and Enhancement of Osteoblast Functions," *Tissue Engineering Part A* 15, no. 2 (2009): 417–426.

291. Z. Zhu, X. Li, Y. Li, et al., "Three-dimensionally Printed Porous Biomimetic Composite for Sustained Release of Recombinant human Bone Morphogenetic Protein 9 to Promote Osteointegration," *Materials & Design* 208 (2021): 109882.

292. S. W. Lee, H. J. Lee, J. W. Lee, et al., "Surface Functionalization of Microgrooved Titanium with Dual Growth Factor-releasing Nanoparticles for Synergistic Osteogenic Differentiation of human Mesenchymal Stem Cells," *Colloids and Surfaces B: Biointerfaces* 135 (2015): 565–574.

293. D. M. Ferris, G. D. Moodie, P. M. Dimond, C. W. D. Giorani, M. G. Ehrlich, and R. F. Valentini, "RGD-coated Titanium Implants Stimulate Increased Bone Formation in Vivo," *Biomaterials* 20, no. 23–24 (1999): 2323–2331.

294. M. Schuler, G. R. H. Owen, D. W. Hamilton, et al., "Biomimetic Modification of Titanium Dental Implant Model Surfaces Using the RGDSP-peptide Sequence: A Cell Morphology Study," *Biomaterials* 27, no. 21 (2006): 4003–4015.

295. J. Guillem-Marti, E. Vidal, A. Girotti, et al., "Functionalization of 3D-Printed Titanium Scaffolds with Elastin-like Recombinamers to Improve Cell Colonization and Osteoinduction," *Pharmaceutics* 15, no. 3 (2023): 872.

296. J. Chen, G. Hu, T. Li, et al., "Fusion Peptide Engineered "Statically-versatile" Titanium Implant Simultaneously Enhancing Anti-infection, Vascularization and Osseointegration," *Biomaterials* 264 (2021): 120446.

297. Y. E. He, C. Mu, X. Shen, et al., "Peptide LL-37 Coating on Microstructured Titanium Implants to Facilitate Bone Formation in Vivo via Mesenchymal Stem Cell Recruitment," *Acta Biomaterialia* 80 (2018): 412–424.

298. M. T. Schwabe and C. P. Hannon, "The Evolution, Current Indications and Outcomes of Cementless Total Knee Arthroplasty," *Journal of Clinical Medicine* 11, no. 22 (2022): 6608.

299. B. Abar, N. Kwon, N. B. Allen, et al., "Outcomes of Surgical Reconstruction Using Custom 3D-Printed Porous Titanium Implants for Critical-Sized Bone Defects of the Foot and Ankle," *Foot & Ankle International* 43, no. 6 (2022): 750–761.

300. C. E. Gross, D. Scott, D. A. Friscia, S. J. Ellis, and R. F. Owens, "A Prospective Evaluation of a 3D-Printed 4th-Generation Total Ankle Prosthesis with 1-Year Follow- Up," *Foot & Ankle Orthopaedics* 9, no. 2 (2024): 44.

301. S. Restrepo, E. B. Smith, and W. J. Hozack, "Excellent Mid-term Follow-up for a New 3D-printed Cementless Total Knee Arthroplasty," *The Bone & Joint Journal* 103-B (2021): 32–37.

302. K. B. Fricka, C. J. McAsey, and S. Sritulanondha, "To Cement or Not? Five-Year Results of a Prospective, Randomized Study Comparing Cemented vs Cementless Total Knee Arthroplasty," *The Journal of Arthroplasty* 34, no. 7 (2019): S183–S187.

303. C. P. Hannon, R. Salih, R. L. Barrack, and R. M. Nunley, "Cementless Versus Cemented Total Knee Arthroplasty," *Journal of Bone and Joint Surgery* 105, no. 18 (2023): 1430–1434.

304. G. Gupta, *OsseoTi^{TM} – Porous Titanium Alloy for Enhanced Bone Integration* (Society for Biomaterials, 2014).

305. E. J. Berlinberg, J. A. Kavian, M. A. Roof, et al., "Minimum 2-Year Outcomes of a Novel 3D-printed Fully Porous Titanium Acetabular Shell in Revision Total Hip Arthroplasty," *Arthroplasty Today* 18 (2022): 39–44.

306. Y. Tamaki, T. Goto, T. Takasago, K. Wada, D. Hamada, and K. Sairyo, "Clinical and Radiological Outcomes of Total Hip Arthroplasty Using a Highly Porous Titanium Cup or a Conventional Hydroxyapatite-coated Titanium Cup: A Retrospective Study in Japanese Patients," *Journal of Orthopaedic Science* 27, no. 1 (2022): 163–168.

307. K. C. McGilvray, J. Easley, H. B. Seim, et al., "Bony Ingrowth Potential of 3D-printed Porous Titanium Alloy: A Direct Comparison of Interbody Cage Materials in an in Vivo Ovine Lumbar Fusion Model," *The Spine Journal* 18, no. 7 (2018): 1250–1260.

308. W. Van Den Brink and N. Lamerigts, "Complete Osseointegration of a Retrieved 3-D Printed Porous Titanium Cervical Cage," *Frontiers in Surgery* 7 (2020): 526020.

309. C. Donaldson, T. Santro, M. Awad, and A. Morokoff, "3D-printed Titanium Alloy Cage in Anterior and Lateral Lumbar Interbody Fusion for Degenerative Lumbar Spine Disease," *Journal of Spine Surgery* 10, no. 1 (2024): 22–29.

310. K. A. Corso, P. Kothari, K. Corrado, A. Michielli, J. Ruppenkamp, and D. Bowden, "Early Revision Events among Patients with a Three

Dimensional (3D) Printed Cellular Titanium or PEEK (polyetheretherketone) Spinal Cage for Single-level Lumbar Spinal Fusion," *Expert Review of Medical Devices* 19, no. 2 (2022): 195–201.

311. E. Marin, S. Fusi, M. Pressacco, L. Paussa, and L. Fedrizzi, "Characterization of Cellular Solids in Ti6Al4V for Orthopaedic Implant Applications: Trabecular Titanium," *Journal of the Mechanical Behavior of Biomedical Materials* 3, no. 5 (2010): 373–381.

312. J. Muth, M. Poggie, G. Kulesha, and R. Michael Meneghini, "Novel Highly Porous Metal Technology in Artificial Hip and Knee Replacement: Processing Methodologies and Clinical Applications," *Jom Journal of the Minerals Metals and Materials Society* 65, no. 2 (2013): 318–325.

313. H. Hothi, J. Henckel, A. Nicum, A. Di Laura, K. Schlueter-Brust, and A. Hart, "Comparative Analysis of Conventionally and Additively Manufactured Acetabular Shells from a Single Manufacturer," *3D Printing in Medicine* 10, no. 1 (2024): 31.

314. R. J. van Arkel, S. Ghouse, P. E. Milner, and J. R. T. Jeffers, "Additive manufactured push-fit implant fixation with screw-strength pull out," *Journal of Orthopaedic Research* 36, no. 5 (2018): 1508–1518.

315. N. Harrison, P. E. McHugh, W. Curtin, and P. Mc Donnell, "Micromotion and Friction Evaluation of a Novel Surface Architecture for Improved Primary Fixation of Cementless Orthopaedic Implants," *Journal of the Mechanical Behavior of Biomedical Materials* 21 (2013): 37–46.

316. N. Ghavidelnia, M. Bodaghi, and R. Hedayati, "Femur Auxetic Meta-Implants with Tuned Micromotion Distribution," *Materials* 14, no. 1 (2020): 114.

317. H. M. A. Kolken, S. Janbaz, S. M. A. Leeflang, K. Lietaert, H. H. Weinans, and A. A. Zadpoor, "Rationally Designed Meta-implants: A Combination of Auxetic and Conventional Meta-biomaterials," *Materials Horizons* 5, no. 1 (2018): 28–35.

318. R. Raj, M. Jiyalal Prajapati, J. T. Tsai, A. Kumar, and J. Y. Jeng, "Design and Additive Manufacturing of Novel Hybrid Lattice Metamaterial for Enhanced Energy Absorption and Structural Stability," *Materials & Design* 245 (2024): 113268.

319. H. Lei, C. Li, X. Zhang, et al., "Deformation Behavior of Heterogeneous Multi-morphology Lattice Core Hybrid Structures," *Additive Manufacturing* 37 (2021).

320. F. Liu, Z. Mao, P. Zhang, D. Z. Zhang, J. Jiang, and Z. Ma, "Functionally Graded Porous Scaffolds in Multiple Patterns: New Design Method, Physical and Mechanical Properties," *Materials & Design* 160 (2018): 849–860.

321. S. Ghanaati, R. E. Unger, M. J. Webber, et al., "Scaffold vascularization in vivo driven by primary human osteoblasts in concert with host inflammatory cells," *Biomaterials* 32, no. 32 (2011): 8150–8160.

322. H. Wang, J. Wu, Y. Chen, et al., "Design of Novel Non-periodic Biomimetic Bone Scaffolds Using the Moving Morphable Components Method," *Materials & Design* 259 (2025): 114815.

323. T. A. Burge, M. J. Munford, S. Kechagias, J. R. T. Jeffers, and C. W. Myant, "Automating the Customization of Stiffness-matched Knee Implants Using Machine Learning Techniques," *The International Journal of Advanced Manufacturing Technology* 126 (2023): 3725–3737.

324. A. Benady, S. J. Meyer, E. Golden, S. Dadia, and G. Katarivas Levy, "Patient-specific Ti-6Al-4V Lattice Implants for Critical-sized Load-bearing Bone Defects Reconstruction," *Materials & Design* 226 (2023): 111605.

325. S. Suvarnapathaki, X. Wu, T. Zhang, et al., "Oxygen Generating Scaffolds Regenerate Critical Size Bone Defects," *Bioactive MaterialsBioactive Materials* 13 (2022): 64–81.

326. D. Shekhawat, A. Singh, A. Bhardwaj, and A. Patnaik, "A Short Review on Polymer, Metal and Ceramic Based Implant Materials," In: IOP Conference Series: Materials Science and Engineering 1017 (IOP Publishing Ltd, 2021): 012038.

327. X. Geng, Y. Li, F. Li, et al., "A New 3D Printing Porous Trabecular Titanium Metal Acetabular Cup for Primary Total Hip Arthroplasty: A Minimum 2-year Follow-up of 92 Consecutive Patients," *J Orthop Surg* 15, no. 1 (2020).

328. H. Liang, J. Tu, B. Wang, et al., "Innovative 3D-printed Porous Tantalum Cage with Non-window Design to Accelerate Spinal Fusion: A Proof-of-concept Study," *Mater Today Bio* 31 (2025): 101576.